ABSTRACT

Title of thesis: STEERING LAWS FOR PURSUIT

Puduru Viswanadha Reddy
Master of Science, 2007

Thesis directed by: Professor P. S. Krishnaprasad
Department of Electrical & Computer Engineering

Dr. Eric W. Justh
Naval Research Laboratory

Pursuit problems have attracted considerable attention from biologists, mathematicians and engineers. Guidance/steering laws are essential in robotic systems. In this thesis, we first review the results on steering laws for a specific pursuit process, motion camouflage with respect to infinity. This type of guidance law renders the baseline (line connecting the pursuer and evader) parallel to a fixed line. In observations of prey pursuit trajectories of echolocating bats, it has been noted that the same geometrical condition of eventual parallelism holds.

We hypothesize that a steering law of the same form as discussed here for motion camouflage with respect to infinity, also applies to the trajectories of prey capture behavior by bats. In this thesis, we develop a method to extract curvatures for trajectories and a detailed investigation to validate this hypothesis. In the latter part of the thesis, we discuss the effect of delays on the performance of motion camouflage laws. We derive limits on the feedback gain and an upper bound on the delay that can be allowed in a pursuit evader system, to ensure successful motion camouflage.

Steering Laws for Pursuit

by

Puduru Viswanadha Reddy

Thesis submitted to the Faculty of the Graduate School of the
University of Maryland, College Park in partial fulfillment
of the requirements for the degree of
Master of Science
2007

Advisory Committee:
Professor P. S. Krishnaprasad, Chair/Advisor
Dr. Eric W. Justh, Co-Advisor
Associate Professor Timothy K. Horiuchi

DEDICATION

to the joy of (restless) inquiry ....

I threw my heart to the winds and followed you.
One day the wind brought me your scent,
my heart swelled in gratitude and scattered in the wind.

— Rumi (1207-73 AD)

ACKNOWLEDGEMENTS

Many thanks to my advisor and teacher, Prof. P. S. Krishnaprasad for giving me freedom and opportunity to work on interesting science problems, for providing generous funding and invaluable advice during difficult times. I have taken four graduate courses in control theory (each with different flavor) with him. I admire his enthusiasm, depth, understanding and personal take on wide variety of topics. Prof. Krishna's uncompromising attitude towards perfection is an inspiration to me. It is indeed a rich learning experience for me working with a true scientist.

I am equally thankful to Dr. Eric Justh for being my co-advisor. Dr. Justh patiently listened my ideas and doubts, gave necessary corrections and thoughtful advice. Dr. Justh was more than willing to spend time given his busy schedule, I cannot realize the results in chapter four without his enthusiasm and timely feedback.

Collaboration with BATLAB was instrumental in shaping out the thesis. I am thankful to Prof. Cynthia Moss and Dr. Kaushik Ghose for sharing ideas and necessary data. I also thank Prof. Timothy Hourichi for serving the thesis committee.

I am grateful to Prof. David L. Elliot for enthusiasm, warmth and advice during necessary times. I thank Prof. Andre Tits for encouragement. I thank Prof. Niranjan Ramachandran for advice and friendship. I am grateful to my teachers at UMD who taught excellent courses and helped improve my understanding. Thanks to Dr. Dan Balon for help during my teaching assistantship days, Maria for help with paperwork and Peg for systems related advice and help.

I am grateful to my friends and labmates - Arash, Bijan, Bargava, Kaushik Mitra, Kevin, Luke, Pratap, Sandy, Srilatha and Vikramjit for warmth and company. Thanks are due to Maben for inspiration and sharing his wisdom, Punya and Punarbasu for friendship and timely help with accommodation. Arun and Vikas were my housemates and often victims to my culinary experiments, I thank them for understanding and company. Special thanks to Arun for general chats and help with computing. Thanks are due to Suresh and Vasundhara who helped me settle

during the initial days. Suresh has been a partner in crime, a good listener and his company taught me few important things in life. I thank my pottery class instructors Peter Holden, who introduced me to the art, and Gina Mai, who honed my skills. Strawberry shakes at Potbelly's, General Tso's Chicken at TenRen's kept my energy levels up at odd hours.

I am grateful to my sister Kala and Pradeep for love and providing me a safe refuge during difficult times. I convey my gratitude to my parents for their selflessness and providing me freedom to pursue my dreams. Thanks to my parent-in-laws for the blessings.

Living in the other side of the planet, my wife Debarupa spent countless hours over telephone patiently listening to my problems. I am extremely thankful to her patience, sacrifice, love and understanding especially during the times when I thought 'I am lost!'. Her unwavering optimism and resilience are a constant source of inspiration to me. 'Debu! thanks for everything!'.

This research was supported in part by the Air Force Office of Scientific Research under AFOSR Grant Nos. FA95500410130 and FA9550710446; by the Army Research Office under ARO Grant No. W911NF0610325; by the Army Research Office under ODDR&E MURI01 Program Grant No. DAAD19-01-1-0465 to the Center for Communicating Networked Control Systems (through Boston University); by NIH-NIBIB grant 1 R01 EB004750-01, as part of the NSF/NIH Collaborative Research in Computational Neuroscience Program.

Table of Contents

List of Tables

List of Figures

Chapter 1

Introduction

Pursuit and interception of moving targets are significant processes in nature and engineering. Animals (predators) pursue and capture prey to acquire food. A few examples are archer fish shooting jets of water at moving insects and bats catching insects in the dark. In sports such as soccer, cricket, frisbee, tennis, etc. humans pursue and intercept moving targets. Military systems such as guided missiles and torpedoes pursue and hit moving targets such as aircraft and ships.

The participants in a pursuit process are pursuer (predator) and evader (prey). The trajectory of a pursuer during a pursuit process could be termed as a pursuit curve. An analytical approach to pursuit problems was started in the eighteenth century by mathematicians studying pursuit curves. Pierre Bouger in 1732 studied the classical pursuit problem, where the pursuer's instantaneous velocity vector is always pointed towards the evader during the pursuit. In classical pursuit the pursuer can intercept the evader only when pursuer's speed is greater than that of evader. Later, the three bug/dog problem was analyzed by H. Brocard in 1877 where each bug/dog chases the next one clockwise or counterclockwise using classical pursuit. Under certain conditions all three bugs/dogs meet at a point called the Brocard point [KN71]. The analysis was later generalized to non symmetric

cases and polygons instead of triangles. This type of pursuit is called cyclic pursuit. Marshall et. al. [MBF04] extend the results of cyclic pursuit when the participants in pursuit are unicycles instead of particles.

In military applications, a pursuit process is termed a guidance process. The applications of guidance are in weaponry which began in 1870 with the invention of guided boat by Werner von Siemens (refer [Shn98] for a detailed historical note). A key objective of the pursuer is to capture the evader. The evader tries to act against the pursuer's objective. If the objective of a guidance process includes active participation of the evader, then optimal steering/guidance laws for such problems are given by game theory. We restrict our attention to the case where the objective involves the pursuer only. The kinematics of the pursuer are modified based on certain rules (or guidance laws) to achieve capture (pursuer's objective). These rules are based on the sensed kinematics of the evader. The classical guidance laws are *Line-of-sight guidance*, *Pure pursuit*, *Parallel navigation*, *Proportional navigation* and *guidance laws related to proportional navigation*. Refer to [Shn98] for a detailed discussion of the above rules. In this thesis we introduce a guidance law for a stealth strategy called *motion camouflage* and it is related to proportional navigation.

1.1 Motion Camouflage (MC)

The term *motion camouflage* originated from the study of stealthy pursuit behaviors in visual insects. In motion camouflage, the pursuer moves in such a way as to mimic the motion of a fixed background object on the retina of the evader,

giving optical cues similar to that of a fixed background object. The pursuer may also move towards or away from the evader along the line joining the pursuer and evader, giving rise to looming cues (i.e., change in size). Equipped with compound eyes, insects such as hoverflies and dragonflies are sensitive to optical flow but not so sensitive to looming. Srinivasan and Davey [SD95] first observed such behaviors in hoverfly trajectories collected by Collett and Land [CL75], and similar behavior was later observed in dragonflies [MCS03].

There are two distinct motion camouflage strategies. In one type of motion camouflage, the pursuer camouflages itself against a fixed background object so that the evader observes no relative motion between the predator and the fixed object. In the other type of motion camouflage, the pursuer approaches the evader such that from the point of view of the evader, the pursuer always appears to be at the same bearing. (In this case, we say that the object against which the pursuer is camouflaged is a point at infinity.)

Srinivasan and Davey [SD95] give two algorithms to achieve motion camouflage. These algorithms require range and optic flow data and are not biologically plausible as it is not clear how dragonflies and hoverflies would extract the required range information. Anderson and McOwan [AM03] propose a bio inspired sensorimotor system using neural networks to achieve motion camouflage. This method uses realistic input information but has drawbacks of a typical neural network (fragile with new test data). In particular, several input output pairs that explore the entire state space are required to train the system, which is prone to failure with

unexpected maneuvers of the evader.

Glendinning [Gle04] modeled motion camouflage trajectories using differential equations. Motion camouflage trajectories were computed for a finite fixed background object and a point at infinity. Further, these studies suggest that motion camouflage is an efficient pursuit strategy compared to classical pursuit. Furthermore, Glendinning's simulations also indicated that capture is possible even when the pursuer moves slower than the evader, in which case classical pursuit simply fails. Carey et. al [CFC04] studied certain cases of motion camouflage as a control problem within a linear gaussian quadratic framework. The main drawback of the work is that the guidance law is derived with the assumption that capture time is known before hand.

Justh and Krishnaprasad [JK06] provide a biologically plausible high gain feedback law to attain a state of motion camouflage with respect to a point at infinity. Pursuer and evader trajectories are modeled using natural frame equations [Bis75]. Further, both pursuer and evader have constant speeds, and evader maneuvers and pursuer controls are possible with steering inputs. A high gain pursuer control law was proposed which is guaranteed to drive the system towards motion camouflage under certain conditions. An infinitesimal characterization of motion camouflage is given, which amounts to requiring that the component of the relative velocity of the evader transverse to the baseline vector (line connecting the evader and pursuer) is equal to zero. This leads to parallelism of the baseline vector when the pursuer-evader system is in a state of motion camouflage. See [RJK06] for the derivation of

motion camouflage feedback laws in 3 dimensions. In this *thesis we only consider the motion camouflage with respect to infinity.* We discuss the results of [RJK06] in chapter 3.

1.2 Constant Absolute Target Direction (CATD)

When the pursuer always moves in such a way as to maintain its bearing (direction of velocity vector) constant, measured with respect to the line joining the pursuer and evader, such a pursuit law is called a constant bearing strategy. Constant bearing (CB) strategy is the time optimal intercept strategy when the evader is moving at constant velocity and the pursuer at constant speed. If the evader is moving erratically then CB is not a time optimal strategy. The pursuer can maintain an optimal bearing if the transverse (to the line joining pursuer and evader) components of the velocity vectors of the pursuer and evader are matched. Then the absolute direction of the line joining them remains constant or the baseline remains parallel, hence the name CATD. See [GHKM06] for a detailed analysis of the CATD strategy. It was observed by [GHKM06] that bats use a CATD strategy to capture the insects.

1.3 Outline of the thesis

In sections (1.1) and (1.2) we reviewed important details about two pursuit strategies, namely, motion camouflage with respect to infinity and CATD. In motion

camouflage (w.r.to infinity) guidance law renders the baseline (line connecting the pursuer and the evader) parallel to a fixed line. It was observed, in [GHKM06], by a detailed experimental study that the echolocating bat uses CATD strategy to capture insects. So, in observations of prey pursuit trajectories by echolocating bat, it has been noted that the same geometrical condition of eventual parallelism holds during the capture phase. Thus motion camouflage and CATD strategies are geometrically indistinguishable. Hence, we hypothesize that a steering law of the same form as discussed here for motion camouflage with respect to infinity, also applies for the trajectories of prey capture behavior by bats. To validate this hypothesis we seek to extract curvatures from bat and insect trajectories.

In chapter 2, we develop tools to extract curvatures from sampled trajectory data. The pursuer and evader trajectories are modeled using natural frames. Using such a generative model we reconstruct the trajectory, extract curvatures and speed information from sampled (at uniform intervals of time) sensor data. Further, we propose a numerically efficient algorithm with good convergence.

In chapter 3, we review results of motion camouflage steering laws mentioned in [RJK06]. The true curvatures are extracted, using the tools developed in chapter 2, for the bat-insect trajectories mentioned in [GHKM06]. Since delays are inevitable due to sensorimotor processing/communication we modify the original hypothesis taking the delays into account. We develop an investigation process to statistically validate the modified hypothesis.

The second part of the thesis is focused on the effect of delays on the performance

of steering laws. Delays in biological systems are mainly due to sensorimotor processing. In engineered systems such as UAVs, mobile robots, guided missiles etc., the guidance laws may be inspired by certain pursuit strategies observed in nature. Sensors are installed on these systems to sense the dynamics of the evader/target. Delays are inevitable in such situations, and are mainly due to signal processing and inherent physics. In chapter 4 we consider the effect of delays on the performance of a specific guidance process, motion camouflage. In particular, we analyze whether it would be possible to drive the pursuer-evader system close to a state of motion camouflage in the presence of delays. To ensure this, we derive bounds on the gain used in the feedback law. We use a planar setting for this analysis, but the 3D case would be straight forward extension.

We conclude the thesis citing possible extensions to the analysis in chapter 5 of the delay problem to 3D.

Chapter 2

Regularized Inversion of Trajectories

2.1 Introduction

In chapter (1) we presented an overview of pursuit strategies, and a particular pursuit strategy called motion camouflage was discussed at length. Almost all the strategies involve estimating the velocity, acceleration by sensing the position/velocity of the evader/target. So, the pursuer steering control generally involves some estimated parameters of the evader. If we need to validate a particular control strategy for a pursuit behavior observed in nature it is important to preserve the inherent geometry while processing the observed (raw) data. In this chapter we first model the observed data using generative models. Further, we propose a numerically efficient regularization method to estimate curvature and speed information from the observations.

2.2 Framed curves

A single particle moving in three dimensional space traces out a trajectory $\gamma : [0, \infty) \rightarrow \mathbb{R}^3$. Let $s(t) = \int_0^t |\dot{\gamma}(\tau)| d\tau$, denote the arc length of the curve from $\gamma(0)$ to $\gamma(t)$. We assume γ to be at least twice continuously differentiable, satisfying,

$\frac{d\gamma}{dt} \neq 0$. Then s is the arc-length parameter of the curve. The speed of the particle is $\frac{ds}{dt} = \nu(t) = ||\dot{\gamma}(t)||$. We call $\gamma(t)$ a *regular curve* if $\dot{\gamma}(t) \neq 0$. For a regular $\gamma(t)$, $s(t)$ is a strict monotone increasing function. The direction of motion of the particle at s is the unit tangent vector to the trajectory, $\mathbf{T}(s) = \gamma'(s) = \frac{d\gamma}{ds}$. We can introduce orthogonal unit vectors which span the space perpendicular to $\mathbf{T}$. Taken together with $\mathbf{T}$, these unit vectors constitute a framing of the curve γ representing the particle trajectory.

For a curve $\gamma(s)$ which is three times continuously differentiable, and for which $\gamma''(s) \neq 0$ for all s, the Frenet-Serret frame ($\mathbf{T},\ \mathbf{N},\ \mathbf{B}$) is uniquely defined. $\mathbf{N}(s)$ is the unit normal vector to the curve γ at s and satisfies $\mathbf{T}(s) = \frac{\frac{d\mathbf{T}(s)}{ds}}{\kappa(s)}$. Where $\kappa(s)$ is called curvature of the curve and is calculated as $\kappa(s) = \left|\frac{d\mathbf{T}(s)}{ds}\right|$. $\mathbf{B}(s)$ is the binormal vector which completes the frame as $\mathbf{B}(s) = \mathbf{T}(s) \times \mathbf{N}(s)$. The Frenet-Serret frame is compactly written as follows:

$$\begin{aligned}
\dot{\gamma}(t) &= \nu(t)\mathbf{T}(t), \\
\dot{\mathbf{T}}(t) &= -\nu(t)\kappa(s(t))\mathbf{N}(t), \\
\dot{\mathbf{N}}(t) &= \nu(t)\kappa(s(t))\mathbf{T}(t) - \tau(s(t))\mathbf{B}(t), \\
\dot{\mathbf{B}}(t) &= \nu(t)\tau(s(t))\mathbf{N}(t). \qquad (2.1)
\end{aligned}$$

The curvature $\kappa(s(t))$ and torsion $\tau(s(t))$ functions are given by expressions involving the derivatives of $\gamma(s)$. We require curvature to be positive and $\kappa(s) = |\gamma''(s)| \neq 0$ to avoid degeneracy in the calculation of $\mathbf{N}(s)$. So, the curve should be atleast three times continuously differentiable.

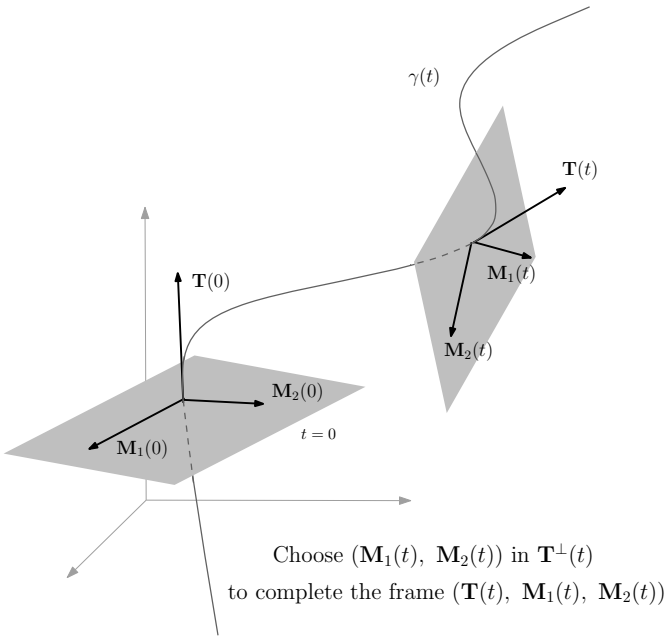

Figure 2.1: Modeling trajectories using natural frames.

Even though the Frenet-Serret frame for a curve is uniquely defined (by the derivatives of the curve), it is not the best choice. In particular, the requirement that $\gamma''(s) \neq 0$ presents serious difficulties for the feedback laws we consider in this thesis. We therefore use an alternative framing of the curve $\gamma(s)$, the natural Frenet frame [Bis75], which is also referred to as the Fermi-Walker frame or Relatively Parallel Adapted Frame (RPAF):

$$\begin{aligned}
\dot{\gamma}(t) &= \nu(t)\mathbf{T}(t), \\
\dot{\mathbf{T}}(t) &= \nu(t)\left(u(t)\mathbf{M}_1(t) + v(t)\mathbf{M}_2(t)\right), \\
\dot{\mathbf{M}}_1(t) &= -\nu(t)u(t)\mathbf{T}(t), \\
\dot{\mathbf{M}}_2(t) &= -\nu(t)v(t)\mathbf{T}(t).
\end{aligned} \tag{2.2}$$

In (2.2), $\mathbf{M}_1(t)$ and $\mathbf{M}_2(t)$ are unit normal vectors which (along with $\mathbf{T}(t)$) complete

a right-handed orthonormal frame (see figure (2.1)). However, there is freedom in the choice of initial conditions $\mathbf{M}_1(0)$ and $\mathbf{M}_2(0)$; once these are specified, the corresponding natural Frenet frame for a twice continuously differentiable curve γ is unique. In this thesis we represent the natural frames $(\mathbf{T}(t),\ \mathbf{M}_1(t),\ \mathbf{M}_2(t))$ as the frame $(\mathbf{x}(t),\ \mathbf{y}(t),\ \mathbf{z}(t))$.

2.3 Problem statement

Given points $\gamma_0,\ \gamma_1,\ \gamma_2,\ \gamma_3,\ \cdots,\ \gamma_N$ in $\mathbb{R}^n$ which are viewed as possibly noisy sample data from a curve, we can reconstruct the curve by using the generative model (2.2) and an optimization criterion. Note that (2.2) is generative in the sense that integrating (2.2) from an initial condition $\gamma(0)$, $\mathbf{x}(0)$, $\mathbf{y}(0)$ and $\mathbf{z}(0)$ yields the curve $\gamma(t)$ and its natural framing. Now, the optimization criterion is given as :

$$\min \left(\underbrace{\sum_{i=0}^{N} |\gamma_i - \gamma(i\delta)|^2}_{I-\text{Fitting Error}} + \underbrace{\lambda \int_0^T (\dot{u}(\sigma)^2 + \dot{v}(\sigma)^2 + \dot{\nu}(\sigma)^2) d\sigma}_{II-\text{Smoothing term}} \right). \tag{2.3}$$

Subject to the constraint $\dot{g}(t) = g(t)\xi(t)$, $g(t) \in SE(3)$ and $\xi(t) \in se(3)$.

$$g(t) = \begin{bmatrix} R(t) & \gamma(t) \\ O & 1 \end{bmatrix},\ R(t) \in SO(3),\ R(t)R^T(t) = I,\ \gamma(t) \in \mathbb{R}^3. \tag{2.4}$$

$$\xi(t) = \begin{bmatrix} \Omega(t) & \mathbf{v}(t) \\ O & 0 \end{bmatrix},\ \Omega(t) \in so(3),\ \Omega(t)^T = -\Omega(t),\ \mathbf{v}(t) \in \mathbb{R}^3 \tag{2.5}$$

λ is the regularization factor which controls the smoothness of the interpolating curve. The curve $\gamma(t)$ is uniquely represented by RPAF $(\mathbf{x}(t),\ \mathbf{y}(t),\ \mathbf{z}(t)))$ with $R(t) = [\mathbf{x}(t),\ \mathbf{y}(t),\ \mathbf{z}(t)]$

$$\Omega(t) = \begin{bmatrix} 0 & -u(t)\nu(t) & -v(t)\nu(t) \\ u(t)\nu(t) & 0 & 0 \\ u(t)\nu(t) & 0 & 0 \end{bmatrix},\ \mathbf{v}(t) = \begin{bmatrix} \nu(t) \\ 0 \\ 0 \end{bmatrix}$$

Terms (I) and (II) in equation (2.3) represent the cost related to fitting error and roughness penalty of the curve respectively. Here the smoothness refers to minimum variation in speed and curvature.

2.4 Solution for the differential equation $\dot{g}(t) = g(t)\xi(t)$

The optimization problem stated above has a differential equation constraint and the differential equation evolves on $SE(3)$. The above constrained problem can be made unconstrained by expressing $\gamma(t)$ explicitly as a function of $u(t)$, $v(t)$ and $\nu(t)$.

Let $h(t) = g^T(t)$, then $\dot{h}(t) = \varphi(t)h(t),$ where $\varphi(t) = \xi^T(t)$. The solution of the system $\dot{h}(t) = \varphi(t)h(t),\ t \in [0,\ T]$, is given by $h(t) = \Phi(t, 0)h(0)$, where $\Phi(t, 0)$ is

expressed as

$$\Phi(t,\tau) = I + \int_{\tau}^{t} \varphi(\sigma_1)d\sigma_1 + \int_{\tau}^{t} \varphi(\sigma_1) \int_{\tau}^{\sigma_1} \varphi(\sigma_2)d\sigma_2 d\sigma_1 + \cdots, \quad t \geq \tau \tag{2.6}$$

So, $g(t) = g(0)\Phi^T(t,0)$. It is very difficult to obtain a closed form solution of $g(t)$ for an arbitrary $\xi(t)$, so numerical methods are used to solve the differential equation. Here, the differential equation evolves over $SE(3)$, so it is highly likely that while solving numerically $g(t_i) \notin SE(3)$, for some $t_i \in [0\ T]$. To address this problem, special methods [Ise02] called *Geometric Integration methods*, which force the solution to stay inside the group $SE(3)$ for all time, are used.

A numerically efficient closed form expression for $g(t)$ is obtained under some assumptions. Consider an uniform partition $\mathcal{P}_K = \{0 = t_0,\ t_1,\ \cdots,\ t_K = T\}$ of the interval $[0,\ T]$, with $t_i - t_{i-1} = \delta\ \forall\ i$, such that $u(.)$, $v(.)$ and $\nu(.)$ are piecewise constant i.e., $u(t) = u_i$, $v(t) = v_i$, $\nu(t) = \nu_i$, then $\varphi(t) = \varphi_i$ (constant matrix) for $t \in [t_{i-1},\ t_i]$.

Using the semi group property of state transition matrix [Bro70] $\Phi(t_m, 0),\ t_m \in [0,\ T]$, $\Phi(t_m, 0)$ can be written as:

$$\Phi(t_m, 0) = \Phi(t_m, t_{m-1})\Phi(t_{m-1}, t_{m-2}) \cdots \Phi(t_1, 0) \tag{2.7}$$

From the piecewise constant curvatures and velocity assumption in the interval $t \in [t_{i-1},\ t_i]$, $\varphi(t) = \varphi_i$. We know $\Phi(t_i, t_{i-1})$ can be expressed as matrix exponential when $\varphi(t)$ is commutative or a constant matrix in $t \in [t_{m-1}\ t_m]$ [Bro70]. Here

$\varphi(t) = \varphi_i$(constant matrix), so $\Phi(t_i, t_{i-1}) = e^{\int_{t_{i-1}}^{t_i} \varphi(\sigma) d\sigma} = e^{\delta\varphi_i}$. As $\varphi_i = \xi_i^T$ and $e^{\delta\xi_i^T} = (e^{\delta\xi_i})^T$ equation (2.7) is given by

$$\begin{aligned} \Phi(t_m, 0) &= e^{\delta\varphi_m} e^{\delta\varphi_{m-1}} \cdots e^{\delta\varphi_1} \\ &= e^{\delta\xi_m^T} e^{\delta\xi_{m-1}^T} \cdots e^{\delta\xi_1^T} \\ &= (e^{\delta\xi_1} e^{\delta\xi_2} \cdots e^{\delta\xi_m})^T \end{aligned} \tag{2.8}$$

Clearly, $\Phi^T(t_m, 0) = e^{\delta\xi_1} e^{\delta\xi_2} \cdots e^{\delta\xi_m}$, so $g(t_m) = g(0) e^{\delta\xi_1} e^{\delta\xi_2} \cdots e^{\delta\xi_m}$. A recursive representation of $g(t_m)$ is given by

$$g(t_m) = g(t_{m-1}) e^{\delta\xi_m} \tag{2.9}$$

REMARK: Here, $\xi_i \in se(3)$, and we know $e^{(\cdot)} : se(3) \to SE(3)$, so $e^{\xi_i} \in SE(3)$. Moreover, the set $SE(3)$ is closed under matrix multiplication, so $g(t_i) \in SE(3)\ \forall\, t_i$. Here,

$$e^{\delta\xi_i} = \begin{bmatrix} cos(\delta\alpha_i\nu_i) & -\frac{u_i}{\alpha_i} sin(\delta\alpha_i\nu_i) & -\frac{v_i}{\alpha_i} sin(\delta\alpha_i\nu_i) & \frac{1}{\alpha_i} sin(\delta\alpha_i\nu_i) \\ \frac{u_i}{\alpha_i} sin(\delta\alpha_i\nu_i) & \frac{v_i^2 + u_i^2 cos(\delta\alpha_i\nu_i)}{\alpha_i^2} & \frac{u_i v_i (cos(\delta\alpha_i\nu_i) - 1)}{\alpha_i^2} & \frac{u_i}{\alpha_i^2}(1 - cos(\delta\alpha_i\nu_i)) \\ \frac{v_i}{\alpha_i} sin(\delta\alpha_i\nu_i) & \frac{u_i v_i (cos(\delta\alpha_i\nu_i) - 1)}{\alpha_i^2} & \frac{u_i^2 + v_i^2 cos(\delta\alpha_i\nu_i)}{\alpha_i^2} & \frac{v_i}{\alpha_i^2}(1 - cos(\delta\alpha_i\nu_i)) \\ 0 & 0 & 0 & 1 \end{bmatrix},$$

and $\alpha_i = \sqrt{(u_i^2 + v_i^2)}$. As $g(t_i) = \begin{bmatrix} R(t_i) & \gamma(t_i) \\ 0 & 1 \end{bmatrix}$, the curve $\gamma(t_k)$ can be repre-

sented recursively as:

$$\gamma(t_i) = \gamma(t_{i-1}) + R(t_{i-1})\Upsilon(t_i), \text{ where } \Upsilon(t_i) = \begin{bmatrix} \frac{1}{\alpha_i} sin(\delta\alpha_i\nu_i) \\ \frac{u_i}{\alpha_i^2}(1 - cos(\delta\alpha_i\nu_i)) \\ \frac{v_i}{\alpha_i^2}(1 - cos(\delta\alpha_i\nu_i)) \end{bmatrix},$$

$$R(t_i) = R(t_{i-1}) \begin{bmatrix} cos(\delta\alpha_k) & -\frac{u_i}{\alpha_i} sin(\delta\alpha_i\nu_i) & -\frac{v_i}{\alpha_i} sin(\delta\alpha_i\nu_i) \\ \frac{u_i}{\alpha_i} sin(\delta\alpha_i\nu_i) & \frac{v_i^2 + u_i^2 cos(\delta\alpha_i\nu_i)}{\alpha_i^2} & \frac{u_i v_i (cos(\delta\alpha_i\nu_i) - 1)}{\alpha_i^2} \\ \frac{v_i}{\alpha_i} sin(\delta\alpha_i\nu_i) & \frac{u_i v_i (cos(\delta\alpha_i\nu_i) - 1)}{\alpha_i^2} & \frac{u_i^2 + v_i^2 cos(\delta\alpha_i\nu_i)}{\alpha_i^2} \end{bmatrix}. \quad (2.10)$$

REMARK: The recursive equation (2.10) is a difference equation with inputs u_i, v_i and ν_i enter the equation in a nonlinear way. Further, the curve $\gamma(t_i)$ is constructed $\forall\ i$ once γ_0 and $R(t_0)$ are known using $\{u_i,\ v_i,\ \nu_i\}$ which is clear from equation (2.10).

2.4.1 Numerical solution of the inputs

Using the piecewise constant assumption for the inputs, the differential equation is solved and a closed form representation for the curve is obtained making the constraints discrete as in (2.10). For this simpler constrained optimization problem the inputs need to be optimized to minimize the modified cost

$$\mathcal{C}(\{(u_i,\ v_i,\ \nu_i)\}) = \textstyle\sum_{j=1}^{N} \mathcal{C}_j \quad (2.11)$$

$$\mathcal{C}_j = |\gamma_j - \gamma(jM)|^2 + \tfrac{\lambda}{\delta^2} \textstyle\sum_{l=(j-1)M+1}^{jM} |u_l - u_{l-1}|^2 + |v_l - v_{l-1}|^2 + |\nu_l - \nu_{l-1}|^2$$

$\mathcal{C}_i$ is the cost associated with reaching γ_i from γ_{i-1}. Let t_{γ_i} be the time instant where γ_i is sampled and let $[t_{\gamma_{i-1}}\ t_{\gamma_i}]$ be partitioned into M equal parts with $t_{\gamma_i} - t_{\gamma_{i-1}} = M\delta$. Clearly for each interval $[t_{\gamma_{i-1}}\ t_{\gamma_i}]$ $3M$ inputs are involved in the optimization, M for each one of the attribute. $(u_i,\ v_i,\ \nu_i)$ are the control inputs needed to move from $\gamma(k-1)$ to $\gamma(k)$, where $k = 1, 2, \cdots, MN$. So, the optimization problem given in (2.3) is modified as finding the minimizer of $\mathcal{C}(\{(u_i,\ v_i,\ \nu_i)\})$. From equation (2.10) it is clear that the curve $\gamma(k)$ can be obtained by specifying the inputs $\{(u_i,\ v_i,\ \nu_i)\}$, initial position, $\gamma(t_0) = \gamma(0)$ and the initial orientation $R(t_0)$. Here $R(t_0)$ is an orthogonal matrix,

$$R(t_0) = \begin{bmatrix} cos(\theta_1) & -sin(\theta_1) & 0 \\ sin(\theta_1) & cos(\theta_1) & 0 \\ 0 & 0 & 1 \end{bmatrix} \begin{bmatrix} cos(\theta_2) & 0 & -sin(\theta_2) \\ 0 & 1 & 0 \\ sin(\theta_2) & 0 & cos(\theta_2) \end{bmatrix} \begin{bmatrix} 1 & 0 & 0 \\ 0 & cos(\theta_3) & -sin(\theta_3) \\ 0 & sin(\theta_3) & cos(\theta_3) \end{bmatrix},$$

which requires $\frac{3(3-1)}{2}$ variables for complete characterization. We thus find that there are $3MN$ variables for inputs and 3 for R_0, so a total of $3MN + 3$ free variables are used in the optimization (2.12).

2.4.2 Initial conditions & implementation

Fitting points by straight lines is the easiest approximation of a curve, and thus the initialization is done by taking the curvatures to be zero. Unit speed initialization is assumed. The unitary matrix R_0 is taken as the product of rotation matrices, which are parameterized by 3 rotation angles, and angles are initialized to zero, leading to $R_0 = I$.

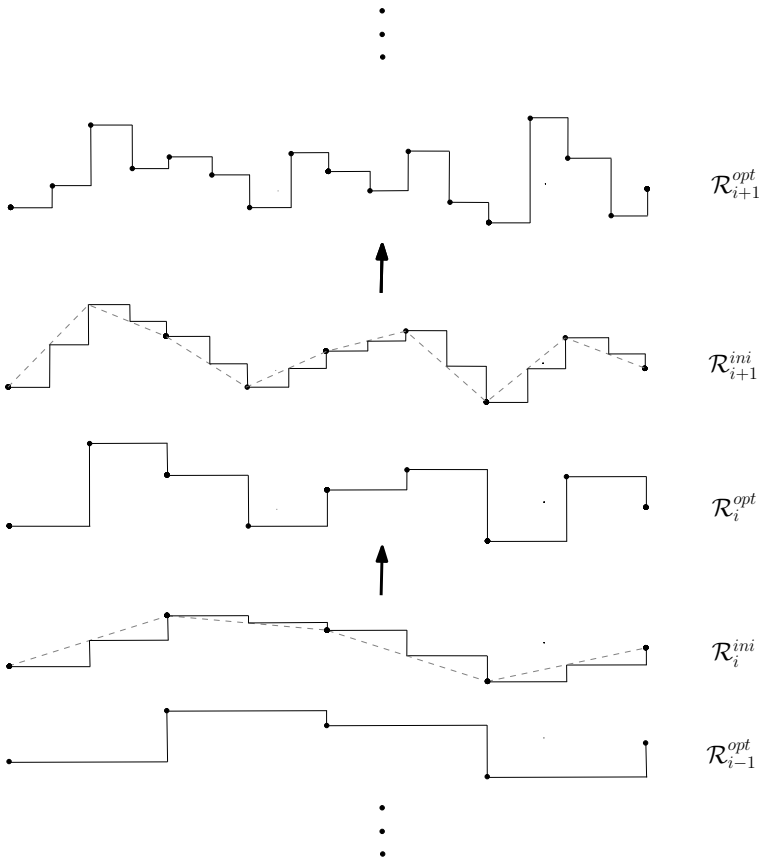

Figure 2.2: Implementation of the optimization algorithm: $\mathcal{R}_{i-1}^{opt}$ represents the optimal set of inputs at $i-1^{th}$ resolution. $\mathcal{R}_{i}^{int}$ represents set of inputs, used for initialization at i^{th} resolution, generated using midpoint rule.

We use a multi resolution approach to achieve fast convergence for the optimization problem. The steps are as follows:

- First sample the data set γ_i's at a coarse resolution.
- Run the optimization routine to arrive at corresponding inputs/controls.
- Interpolate the optimized inputs using midpoint rule, use this input set as an initial sequence for optimizing a data set with higher resolution.
- Repeat this process till all the points in the data set are used.

Figure (2.2) schematically illustrates optimization process. Clearly, this algorithm is sub frame adaptable. The MATLAB optimization routine *fminunc* is used to solve the optimization problem.

2.5 Examples

2.5.1 Circular helix $\gamma(t) = (rcos(wt),\ rsin(wt),\ hwt) \quad 0 \leq t \leq 1.$

A circular helix is parameterized with 2 parameters r, h and $w = \frac{1}{\sqrt{(r^2+h^2)}}$. Here $r = 0.2$ and $h = 0.25$ are considered. The resulting circular helix is given in figure (2.3). The circular helix is sampled uniformly with $N = 75$ points (shown as dots in figure (2.3)). With $M = 1$, the inputs $\{(u_i,\ v_i,\ \nu_i)\}$ are specified at 75

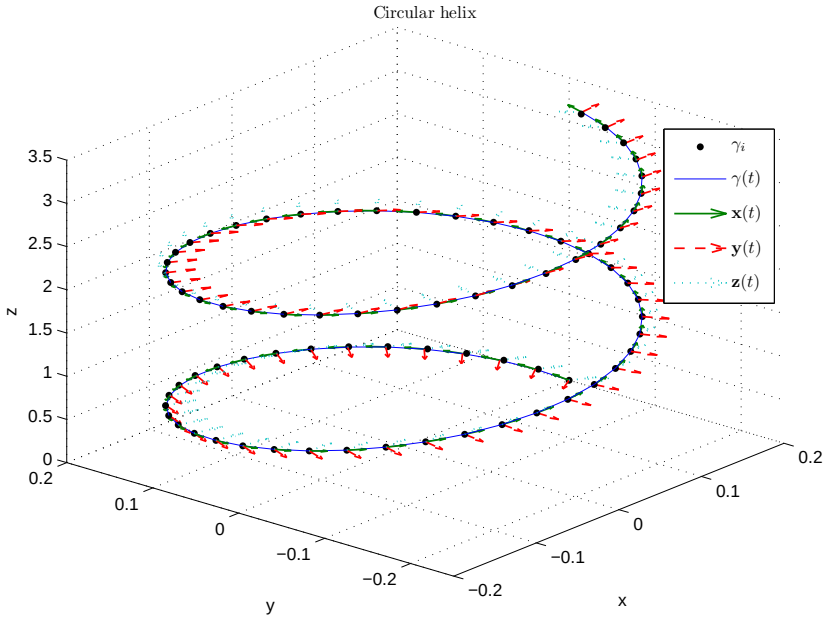

Figure 2.3: Circular helix with $r = 0.2$ and $h = 0.25$: Dots represent the sampled points on helix. Solid curve represents the reconstructed helix using regularized inversion algorithm and the arrows represent natural frame.

points. $u - v$ plot is shown in figure (2.4). Similarly for $M = 2$ and $M = 4$ the inputs were calculated and the corresponding $u - v$ plots are shown in figures (2.5) and (2.6) respectively.

REMARK: It is observed that as the regularization parameter λ is increased the

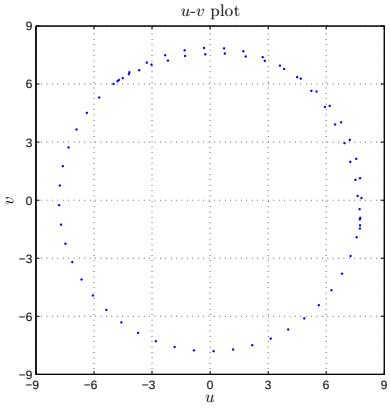

Figure 2.4: $u - v$ plot with $N = 75, M = 1, \lambda = 0.001, r_{est} = 0.1871, h_{est} = 0.2486$

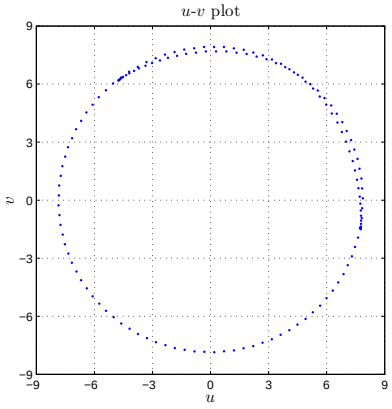

Figure 2.5: $u - v$ plot with $N = 75, M = 2, \lambda = 0.001, r_{est} = 0.1889, h_{est} = 0.2493$

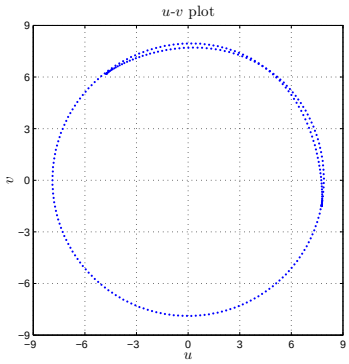

Figure 2.6: $u - v$ plot with $N = 75, M = 4, \lambda = 0.01, r_{est} = 0.1850, h_{est} = 0.2496$

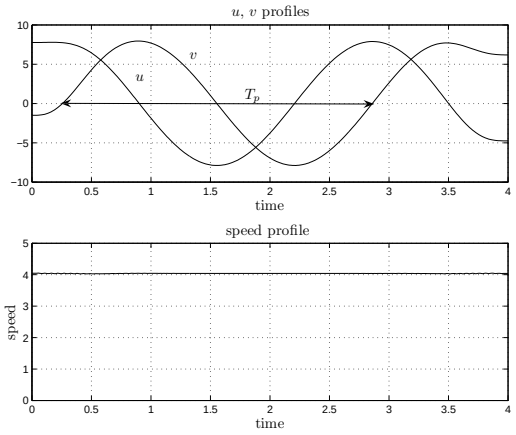

Figure 2.7: Speed (ν) and curvature (u and v) profiles for $N = 75, M = 4$

u and v profiles get smoother. A large increase in λ results in poor interpolation performance. After some trial and error $\lambda = 0.01$ seems to be a good choice. Further, for good convergence a small value of λ is chosen first and it is increased till a good compromise of fitting error and smoothness is obtained. The speed profiles for all the cases is observed to be a constant function. Refer to figure (2.7) for curvature and speed profiles.

Estimation of helix parameters:

The helix parameters are estimated from the attributes as follows: We know, analytically, that u, v satisfy an equation of a circle when $\gamma(t)$ is a circular helix, with $u(t) = -w^2 r sin(w^2 ht)$ and $v(t) = -w^2 r cos(w^2 ht)$. Let r_{est} and h_{est} be the estimates of r and h for the helix. From the observations u_i, v_i the estimates are calculated as:

$$\begin{aligned} \frac{r_{est}}{r_{est}^2 + h_{est}^2} &= \sqrt{\frac{1}{NM}\sum_{i=1}^{NM} u_i^2 + v_i^2}, \\ \frac{h_{est}}{r_{est}^2 + h_{est}^2} &= \frac{2\pi}{T_p}. \end{aligned}$$

Here r_{est} is an MMSE estimate. T_p is the time to second repetition of a value in the $u_i,\ v_i$ profiles. As the inputs are discrete, the repetition may not be exact, a small deviation is allowed. It is observed that boundaries of u, v profiles deviate slightly from the expected profiles, and this could be a reason for inconsistency in the estimates of r. Refer to figures (2.4), (2.5) and (2.6) for estimates r_{est} and h_{est} for different cases.

2.5.2 Circular helix + noise

The optimization routine has also been tested on noisy data. A circular helix of 3 turns is assumed and a gaussian noise with zero mean and variance of 0.01 is added to this helix data, shown in figure (2.8). Here $N = 75$ and 3 cases $M = 1, 2, 4$ are

considered. The regularization parameter is first taken as $\lambda = 0.0001$ and increased to $\lambda = 0.01$. Figures (2.9-2.11) illustrate u-v plots for the three cases. We observe distortion in u-v plot due to noise.

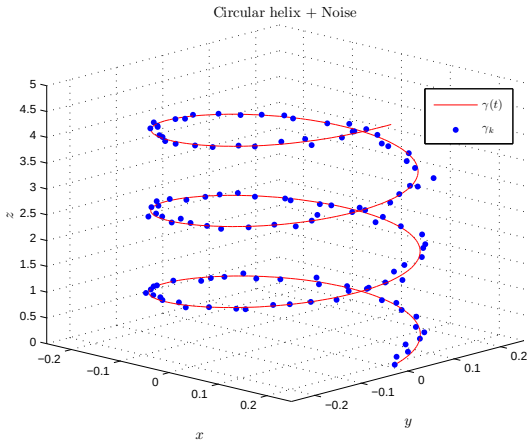

Figure 2.8: Circular helix plus noise

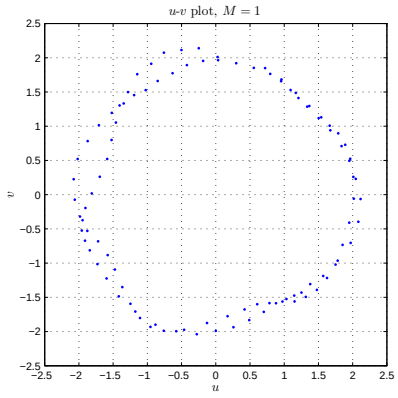

Figure 2.9: $u - v$ plot with $N = 75, M = 1, \lambda = 0.01$

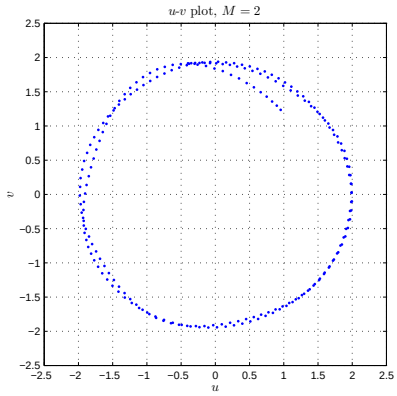

Figure 2.10: $u - v$ plot with $N = 75, M = 2, \lambda = 0.01$

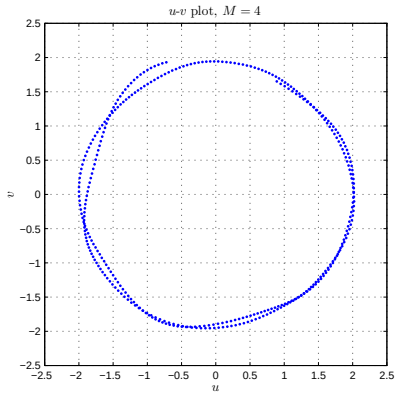

Figure 2.11: $u - v$ plot with $N = 75, M = 4, \lambda = 0.01$

2.5.3 Curve on the sphere $x^2 + y^2 + z^2 = 100$:

$\gamma(t)$ is taken as a curve on a sphere $x^2 + y^2 + z^2 = 100$. The curve, as shown in figure (2.12), is generated as $\gamma(t) = (x(t),\ y(t),\ z(t))$, $x(t) = t$, $y(t) = t^2$ and

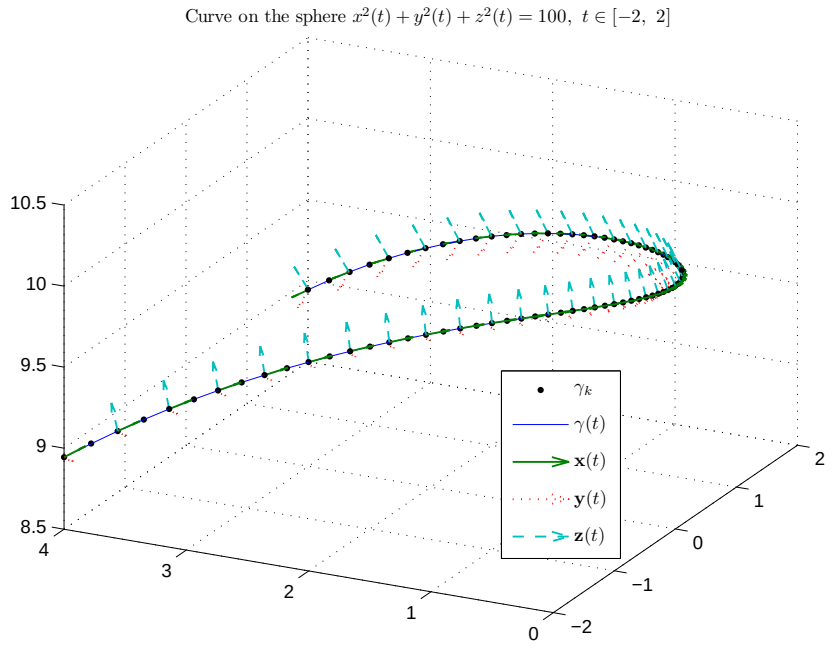

Figure 2.12: Curve on the sphere $x^2 + y^2 + z^2 = 100$. Dots represent the sampled points on sphere. The solid line represents reconstructed curve using regularized inversion algorithm and the arrows represent natural frame.

$z(t) = \sqrt{100 - x^2(t) - y^2(t)}$ with $t \in [-2,\ 2]$. We know from frame theory (with natural frames), that for such a curve the curvatures $u(t)$ and $v(t)$ form a straight line in $u - v$ plane which is away from the origin and the perpendicular distance from the origin is $\frac{1}{R}$, where R is the radius of the sphere. $\gamma(t)$ is sampled uniformly with $N = 44$ points. The optimization is done for $M = 2, 4$ cases. Here the regularization parameter λ is taken as 0.0001 then increased till 0.01. We observed that $\lambda = 0.01$ gives a satisfactory tradeoff for fitting and smoothness performance. Figures (2.13) and (2.14) show the curvature and speed profiles respectively.

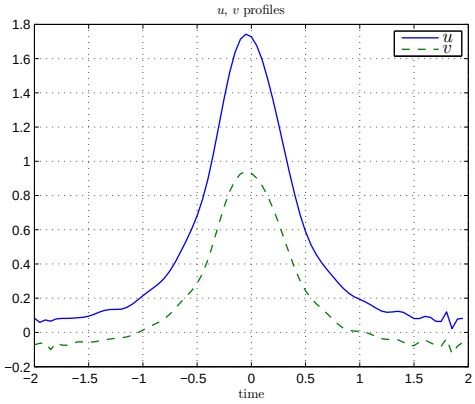

Figure 2.13: u, v profiles – $N = 44, M = 2$

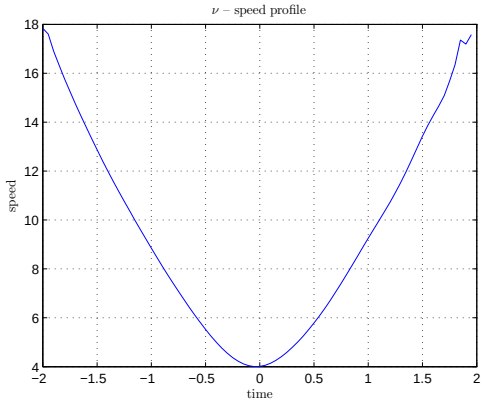

Figure 2.14: Speed profile $N = 44, M = 2$

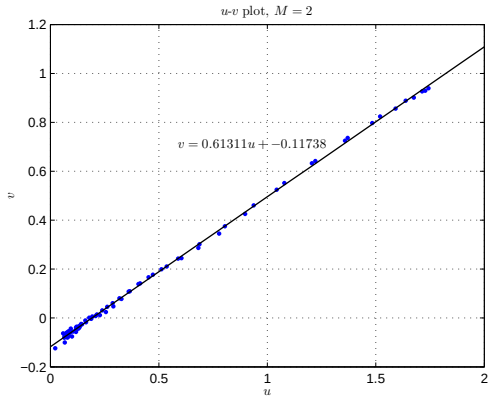

Figure 2.15: Leastsquares line fit $v = 0.6131u - 0.1174$. $\sigma^2_{esterr} = 2.9288\text{e-}3$, $R_{est} = 9.9927$

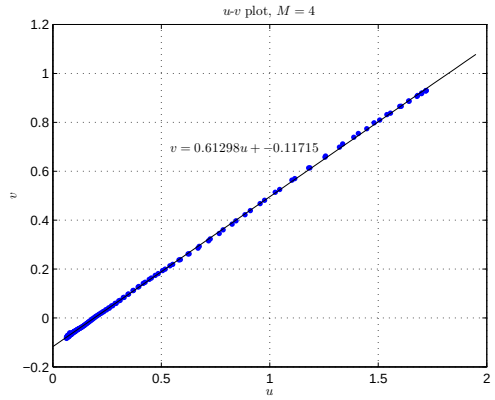

Figure 2.16: Least squares line fit $v = 0.6130u - 0.1172$, $\sigma^2_{esterr} = 4.2907\text{e-}4$, $R_{est} = 10.0121$

R_{est} from the inputs

We know for a curve on the sphere $x^2 + y^2 + z^2 = R^2$, $\{u, v\}$ satisfy the equation $v = mu + c$ and $R = \frac{\sqrt{m^2+1}}{c}$. From the optimized inputs $\{u_i,\ v_i,\ \nu_i\}$, a linear lest squares fit the above form is obtained. An estimate of the radius is given by

$$R_{est} = \frac{\sqrt{m_{est}^2 + 1}}{|c_{est}|}, \text{ with } \begin{bmatrix} NM & \sum_{i=1}^{NM} k_{1i} \\ \sum_{i=1}^{NM} k_{1i} & \sum_{i=1}^{NM} k_{1i}^2 \end{bmatrix} \begin{bmatrix} c_{est} \\ m_{est} \end{bmatrix} = \begin{bmatrix} \sum_{i=1}^{NM} k_{2i} \\ \sum_{i=1}^{NM} k_{1i} k_{2i} \end{bmatrix} \quad (2.12)$$

The estimation error is given as $\sigma^2_{esterr} = \frac{1}{M}\sum_i(|v_i - m_{est}u_i - c_{est}|^2)$. Figures (2.15) and (2.16) show the linear fits and estimates R_{est} and σ^2_{esterr} for $M = 2,\ 4$ respectively.

2.5.4 Bat mantis data

Neuroethology is a branch of science that seeks to understand the neural basis of natural animal behavior. There has been a long standing interest to learn how bats and dolphins use SONAR to locate their prey. The motivation behind this work is to observe the control laws used by a bat while following its prey. Several experiments were conducted at The Auditory Neuroethology Laboratory [1] (BATLAB for short), with mantis as a prey. For the current problem, trials where bat eventually catches the mantis were used.

Here the optimization is done with $M = 4$. Figure (2.17) show Bat-Mantis trajectories where the bat eventually catches the mantis and figures (2.18) show the corresponding curvature and velocity profiles for the Bat-Mantis trajectories, obtained using Natural Frames.

[1]Department of Psychology, University of Maryland Collage Park, USA.

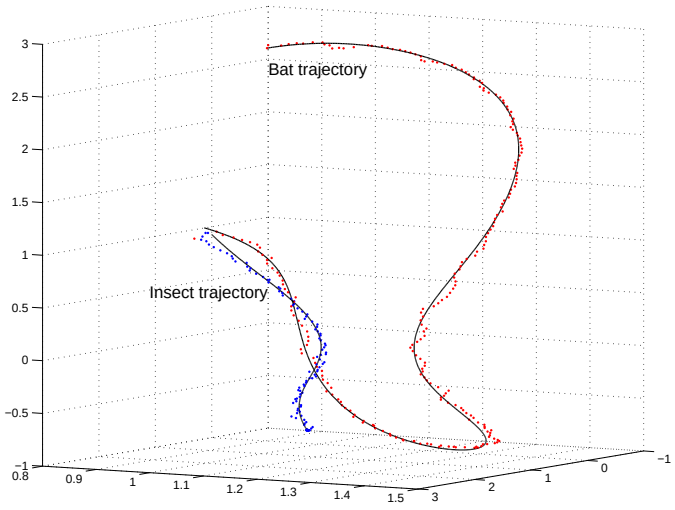

Figure 2.17: Bat and mantis trajectories for data set `MANTMNO2VP-22`. The dotted lines represent noisy sampled data and the black solid line represents reconstructed trajectory.

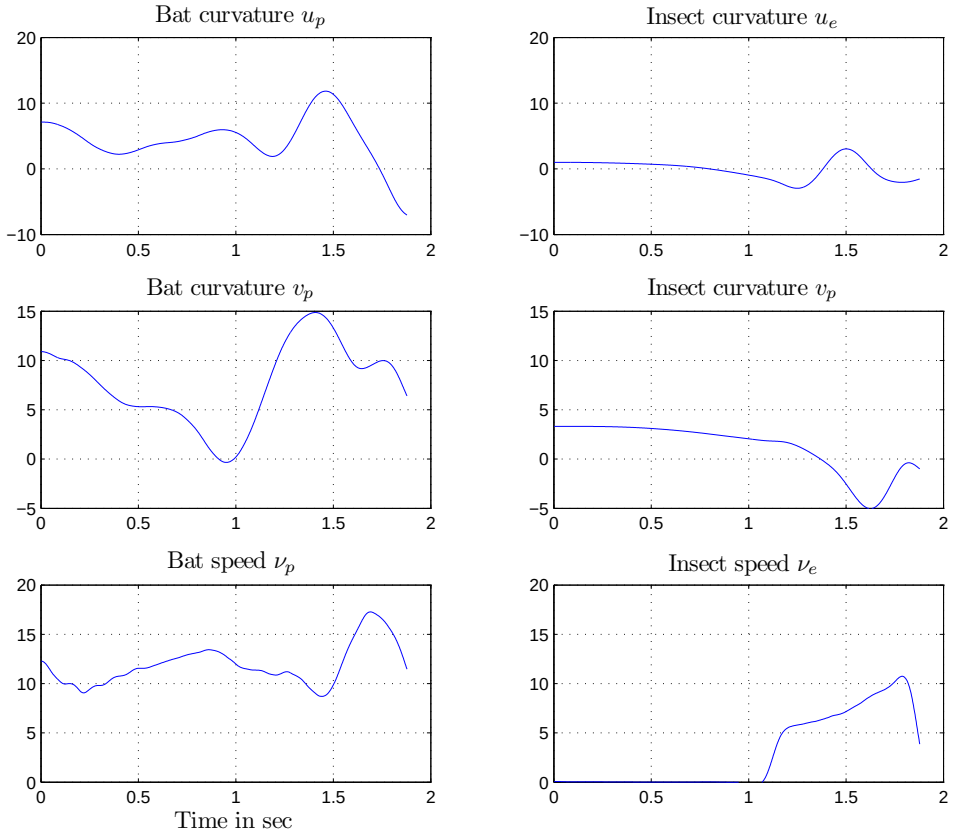

Figure 2.18: Curvature and speed profiles of bat and mantis trajectories for data set `MANTMNO2VP-22`.

Chapter 3

Statistical Analysis of MC Feedback Laws

3.1 Introduction

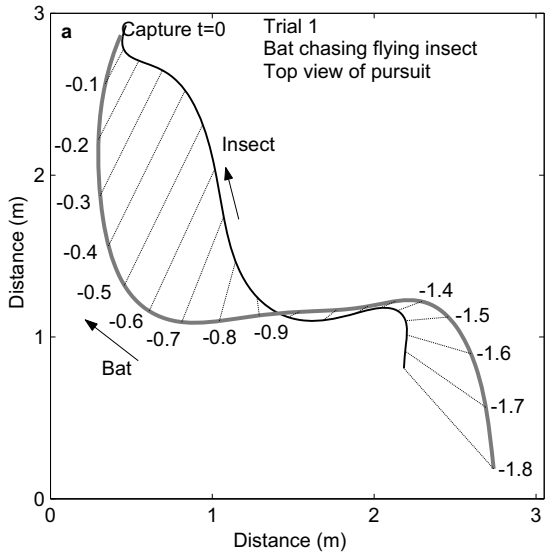

Figure 3.1: Baseline connecting the bat and insect remains parallel for nearly 0.6 sec before the capture (reproduced from [GHKM06]).

Studies in behavioral neuroscience [GHKM06] have shown that for targets moving in a straight line or in a predictable trajectory, constant bearing is the optimal intercept strategy. For targets moving in unpredictable fashion or making fast maneuvers, constant absolute target direction (CATD) strategy appears to be a nearly time optimal strategy. From figure (3.1) it is clearly seen that the line joining the bat and insect remains parallel (baseline parallelism). In chapter (1), we intro-

duced the notion of motion camouflage and the underlying control/steering laws that drive the system to the state of motion camouflage in a finite time. Strikingly the motion camouflage trajectories are geometrically indistinguishable from the bat - insect trajectories near the capture region (400 ms before capture happens [GHKM06]). This naturally leads to a hypothesis: feedback/steering laws for motion camouflage given in [RJK06] should be supported by bat - insect trials discussed in [GHKM06]. To be precise, the above geometrical similarity predicts a linear relation between hypothesized curvatures (motion camouflage) and true curvatures in the bat - insect trials. We use regularized inversion algorithm, discussed at length in chapter (2), to extract the true curvatures. In this chapter we execute a detailed statistical analysis to verify the hypothesis.

3.2 Motion camouflage model

We model the pursuer and evader as point particles, and use natural frames and curvature controls to describe their motion in $\mathbb{R}^3$. We consider the problem of motion camouflage in which the pursuer (predator) tries to intercept the evader (prey) while appearing to the prey as though it is always at the same bearing (i.e., motion camouflaged against the point at infinity). The dynamics of the pursuer and evader are given by

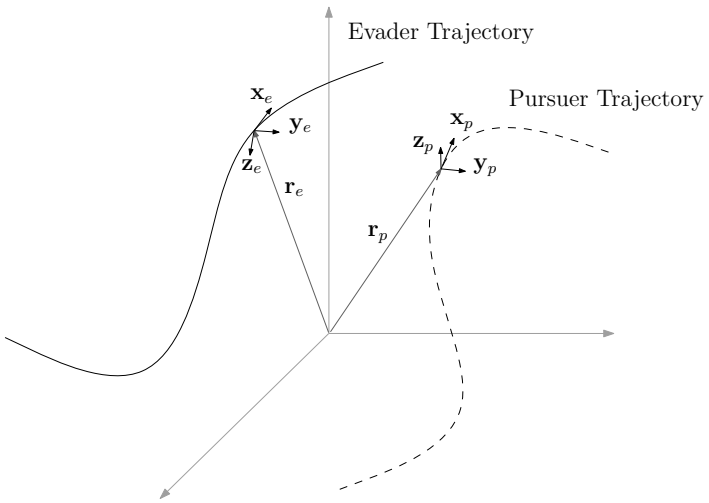

Figure 3.2: Pursuer evader trajectories modeled using natural frames

$$
\begin{aligned}
\dot{\mathbf{r}}_p &= \nu_p \mathbf{x}_p, \\
\dot{\mathbf{x}}_p &= \nu_p(\mathbf{y}_p u_p + \mathbf{z}_p v_p), \\
\dot{\mathbf{y}}_p &= -\nu_p \mathbf{x}_p u_p, \\
\dot{\mathbf{z}}_p &= -\nu_p \mathbf{x}_p v_p, \qquad (3.1) \\
\dot{\mathbf{r}}_e &= \nu_e \mathbf{x}_e, \\
\dot{\mathbf{x}}_e &= \nu_e(\mathbf{y}_e u_e + \mathbf{z}_e v_e), \\
\dot{\mathbf{y}}_e &= -\nu_e \mathbf{x}_e u_e, \\
\dot{\mathbf{z}}_e &= -\nu_e \mathbf{x}_e v_e, \qquad (3.2)
\end{aligned}
$$

where $\mathbf{r}_p$ ($\mathbf{r}_e$) is the position of the pursuer (evader), ν_p (ν_e) is the speed of the pursuer (evader), $\mathbf{x}_p$ ($\mathbf{x}_e$) is the unit tangent vector to the trajectory of the pursuer (evader), $\mathbf{y}_p$ ($\mathbf{y}_e$) and $\mathbf{z}_p$ ($\mathbf{z}_e$) span the normal plane to $\mathbf{x}_p$ ($\mathbf{x}_e$) (completing a right-handed orthonormal basis with $\mathbf{x}_p$ ($\mathbf{x}_e$)), and the natural curvatures u_p (u_e) and v_p (v_e) are the controls for the pursuer (evader). Figure (3.2) illustrates equations (3.1) and (3.2). Note that $\{\mathbf{x}_p,\ \mathbf{y}_p,\ \mathbf{z}_p\}$ and $\{\mathbf{x}_e,\ \mathbf{y}_e,\ \mathbf{z}_e\}$ are natural Frenet frames

for the trajectories of the pursuer and evader.

3.2.1 Characterizing motion camouflage

For motion camouflage with respect to the point at infinity, the pursuer evader trajectories should satisfy (as given in [JK06])

$$\mathbf{r}_p = \mathbf{r}_e + \lambda \mathbf{r}_\infty \tag{3.3}$$

where $\mathbf{r}_\infty$ is a fixed unit vector and λ is a time-dependent scalar. Here $\mathbf{r}_\infty$ represents a particular motion camouflage state. Let

$$\mathbf{r} = \mathbf{r}_p - \mathbf{r}_e \tag{3.4}$$

be the vector from the evader to the pursuer. We refer to $\mathbf{r}$ as the baseline vector, and $|\mathbf{r}|$ as the baseline length. We restrict attention to non-collision states, i.e., $\mathbf{r} \neq 0$. In that case, the component of the pursuer velocity $\mathbf{r}_p$ transverse to by the baseline is

$$\dot{\mathbf{r}}_p - \left(\frac{\mathbf{r}}{|\mathbf{r}|} \cdot \dot{\mathbf{r}}_p \right) \frac{\mathbf{r}}{|\mathbf{r}|}, \tag{3.5}$$

and similarly, that of the evader is

$$\dot{\mathbf{r}}_e - \left(\frac{\mathbf{r}}{|\mathbf{r}|} \cdot \dot{\mathbf{r}}_e \right) \frac{\mathbf{r}}{|\mathbf{r}|}. \tag{3.6}$$

The relative transverse component is

$$\mathbf{w} = (\dot{\mathbf{r}}_p - \dot{\mathbf{r}}_e) - \left(\frac{\mathbf{r}}{|\mathbf{r}|} \cdot (\dot{\mathbf{r}}_p - \dot{\mathbf{r}}_e)\right) \frac{\mathbf{r}}{|\mathbf{r}|} = \dot{\mathbf{r}} - \left(\frac{\mathbf{r}}{|\mathbf{r}|} \cdot \dot{\mathbf{r}}\right) \frac{\mathbf{r}}{|\mathbf{r}|}. \tag{3.7}$$

Lemma [JK06] (Infinitesimal characterization of motion camouflage): The pursuit-evasion system (3.1), (3.2) is in a state of motion camouflage without collision on an interval iff $\mathbf{w} = 0$ on that interval.

Proof: For the if part, suppose motion camouflage holds. Then

$$\mathbf{r}(t) = \lambda(t)\mathbf{r}_\infty, \quad \forall t \in [0,\ T] \tag{3.8}$$

Differentiating the above equation we have, $\dot{\mathbf{r}}(t) = \dot{\lambda}(t)\mathbf{r}_\infty$. Hence,

$$\mathbf{w} = \dot{\mathbf{r}} - \left(\frac{\mathbf{r}}{|\mathbf{r}|} \cdot \dot{\mathbf{r}}\right) \frac{\mathbf{r}}{|\mathbf{r}|} = \dot{\lambda}\mathbf{r}_\infty - \left(\frac{\lambda}{|\lambda|}\frac{\mathbf{r}_\infty}{|\mathbf{r}_\infty|} \cdot \lambda\mathbf{r}_\infty\right) \frac{\lambda}{|\lambda|}\frac{\mathbf{r}_\infty}{|\mathbf{r}_\infty|} = 0 \tag{3.9}$$

For only if part, suppose $\mathbf{w} = 0$ then, $\dot{\mathbf{r}} = \left(\frac{\mathbf{r}}{|\mathbf{r}|} \cdot \dot{\mathbf{r}}\right) \frac{\mathbf{r}}{|\mathbf{r}|} = \xi(t)\mathbf{r}(t)$. So,

$$\mathbf{r}(t) = |\mathbf{r}(0)| \left(\int_0^t \xi(\sigma)d\sigma\right) \frac{\mathbf{r}(0)}{|\mathbf{r}(0)|} = \lambda(t)\mathbf{r}_\infty \tag{3.10}$$

where $\lambda(t) = |\mathbf{r}(0)| \left(\int_0^t \xi(\sigma)d\sigma\right)$ and $\mathbf{r}_\infty = \frac{\mathbf{r}(0)}{|\mathbf{r}(0)|}$. $\square$

3.2.2 Measuring departure from motion camouflage

Consider the ratio

$$\Gamma(t) = \frac{\frac{d}{dt}|\mathbf{r}|}{\frac{d\mathbf{r}}{dt}}, \tag{3.11}$$

which compares the rate of change of the baseline length to the absolute rate of change of the baseline vector. If the baseline experiences pure lengthening (shortening), then the ratio assumes its maximum (minimum) value, $\Gamma(t) = 1$ (-1). $\Gamma = 0$ corresponds to pure rotation of the baseline vector.

$$\frac{d}{dt}|\mathbf{r}| = \frac{\mathbf{r}}{|\mathbf{r}|} \cdot \dot{\mathbf{r}}, \tag{3.12}$$

we see that $\Gamma(t)$ can be written as

$$\Gamma(t) = \frac{\mathbf{r}}{|\mathbf{r}|} \cdot \frac{\dot{\mathbf{r}}}{|\dot{\mathbf{r}}|} \tag{3.13}$$

From

$$|\mathbf{w}|^2 = |\dot{\mathbf{r}}|^2 - \left(\frac{\mathbf{r}}{|\mathbf{r}|} \cdot \dot{\mathbf{r}}\right)^2 = |\dot{\mathbf{r}}|^2 \left(1 - \Gamma^2\right) \tag{3.14}$$

it follows that $(1 - \Gamma^2)$ is a measure of departure from motion camouflage. So, we seek to derive steering laws for the pursuer that drive $\Gamma(t)$ close to -1, which is ensured if $\dot{\Gamma} \leq 0$.

3.2.3 Feedback law and interpretation

Before analyzing $\dot{\Gamma}$ we take a small deviation and write $\mathbf{w}$ as

$$\begin{aligned} \mathbf{w} &= \dot{\mathbf{r}}\left(\frac{\mathbf{r}}{|\mathbf{r}|}\cdot\frac{\mathbf{r}}{|\mathbf{r}|}\right) - \frac{\mathbf{r}}{|\mathbf{r}|}\left(\frac{\mathbf{r}}{|\mathbf{r}|}\cdot\dot{\mathbf{r}}\right) = \frac{\mathbf{r}}{|\mathbf{r}|}\times\left(\dot{\mathbf{r}}\times\frac{\mathbf{r}}{|\mathbf{r}|}\right) \\ \mathbf{w}\times\frac{\mathbf{r}}{|\mathbf{r}|} &= \dot{\mathbf{r}}\times\frac{\mathbf{r}}{|\mathbf{r}|} \end{aligned}$$

$\dot{\mathbf{r}}\times\frac{\mathbf{r}}{|\mathbf{r}|}$ is a biologically plausible quantity to appear in a feedback law, since it only requires sensing $\mathbf{w}$ and $\frac{\mathbf{r}}{|\mathbf{r}|}$. The quantity $\left(\dot{\mathbf{r}}\times\frac{\mathbf{r}}{|\mathbf{r}|}\right)$ can be interpreted in terms of an angular-velocity-like quantity. From the point of view of the pursuer, consider an extensible rod connecting the pursuer and evader positions. The motion of the evader (relative to the pursuer) contributes to change in the length of this rod, as well as to angular velocity of the rod. The transverse component of the velocity of the evader (viewed from the pursuer) is simply (as in equation (3.7))

$$\mathbf{w} = (\dot{\mathbf{r}}_p - \dot{\mathbf{r}}_e) - \left[(\dot{\mathbf{r}}_p - \dot{\mathbf{r}}_e)\cdot\frac{\mathbf{r}_p - \mathbf{r}_e}{|\mathbf{r}_p - \mathbf{r}_e|}\right]\frac{\mathbf{r}_p - \mathbf{r}_e}{|\mathbf{r}_p - \mathbf{r}_e|} \tag{3.15}$$

which can also be expressed as

$$-\mathbf{w} = \omega\times(-\mathbf{r})\,, \tag{3.16}$$

where ω is the angular velocity of the rod. Clearly, using cross product manipulations we can write ω as

$$\omega = \frac{\mathbf{r}}{|\mathbf{r}|^2}\times\dot{\mathbf{r}} \tag{3.17}$$

Thus $\dot{\mathbf{r}} \times \frac{\mathbf{r}}{|\mathbf{r}|}$ is simply $-\omega$ scaled with $|\mathbf{r}|$. For convenience in the calculations below, we define

$$\mathbf{a} = \mathbf{x}_p \times \left(\dot{\mathbf{r}} \times \frac{\mathbf{r}}{|\mathbf{r}|} \right) \tag{3.18}$$

and express the feedback laws as

$$u_p = \mu(\mathbf{a} \cdot \mathbf{y}_p), \tag{3.19}$$

$$v_p = \mu(\mathbf{a} \cdot \mathbf{z}_p) \tag{3.20}$$

where $\mu > 0$ is a constant feedback gain. This particular choice of steering laws facilitate in cancelation of terms while analyzing the behavior of $\dot{\Gamma}$. A detailed analysis is given in section (III.B) of [RJK06]. Again using cross product identities we can write

$$u_p = -\mu \left[\left(\dot{\mathbf{r}} \times \frac{\mathbf{r}}{|\mathbf{r}|} \right) \cdot \mathbf{z}_p \right], \tag{3.21}$$

$$v_p = \mu \left[\left(\dot{\mathbf{r}} \times \frac{\mathbf{r}}{|\mathbf{r}|} \right) \cdot \mathbf{y}_p \right] \tag{3.22}$$

Using the above feedback laws motion camouflage can be attained in finite time under certain conditions. We state a theorem without proof (refer [RJK06] for a detailed proof).

Proposition: Consider the system (3.1) and (3.2) with Γ defined by (3.13) and control law given by (3.21) - (3.22), with the following hypotheses:

(A1) $0 < \nu_p^{low} < \nu_p < \nu_p^{high}$ where ν_p^{low} and ν_p^{high} are constants,

(A2) $0 < \nu_e^{low} < \nu_e < \nu_e^{high}$ where ν_e^{low} and ν_e^{high} are constants,

(A3) $\frac{\nu_e}{\nu_p} \leq \nu_{max} < 1$, where ν_{max} is constant,

(A4) where u_e and v_e are piecewise continuous and $\sqrt{u_e^2 + v_e^2}$ is bounded,

(A5) $\dot{\nu}_p$ and $\dot{\nu}_e$ are piecewise continuous, $|\dot{\nu}_p| < \alpha_p$, and $|\dot{\nu}_e| < \alpha_e$, where α_p and α_e are finite constants,

(A6) $\Gamma_0 = \Gamma(0) < 1$ and

(A7) $|\mathbf{r}(0)| > 0$.

Motion camouflage is accessible in finite time using high gain feedback (i.e., by choosing $\mu > 0$ sufficiently large).

3.3 Feedback law leads to a hypothesis

We discussed in section (3.1) that the trajectories of the pursuer-evader system are geometrically indistinguishable with CATD and motion camouflage (with respect to a fixed object at infinity) strategies. So we hypothesize that the proportional feedback laws, that drive the system to a state of motion camouflage in finite time, should be supported by bat insect trials mentioned in [GHKM06]. We write the scaled proportional feedback laws as follows:

$$\begin{aligned} \hat{u}_p &= -\left[\left(\dot{\mathbf{r}} \times \frac{\mathbf{r}}{|\mathbf{r}|}\right) \cdot \mathbf{z}_p\right] \\ \hat{v}_p &= \left[\left(\dot{\mathbf{r}} \times \frac{\mathbf{r}}{|\mathbf{r}|}\right) \cdot \mathbf{y}_p\right] \end{aligned} \tag{3.23}$$

3.3.1 Role of delay

The echolocating bat such as *Eptesicus fuscus* produces high frequency ultrasonic pulses, which upon echo, give an acoustic image of the surroundings. Using such a sensing mechanism bats perform complex tracking behaviors to catch the prey. There is an inevitable delay due to the cumulative effect of sensory motor processing (in bat) and acoustic delay of the ultrasound pulses. Further, from [GM06] the pulse production rate (PPR) during the capture phase amounts to an acoustic delay of 10ms. In the statistical study that follows we let the combined delay be δ, and find the best δ that explains the data.

The proportional feedback laws are designed to act instantaneously. Since there is a delay due to sensorimotor processing and acoustic delay, the hypothesis is modified to incorporate delays in the feedback laws. The feedback laws can take various forms with the incorporation of delays. The feedback could be of a preprocessing type where the bat predicts the possible control to be applied, similar to the control law given by [MS] in a tracking with delay context. We assume a simple model where bat uses a delayed version of the proportional feedback law. So, we hypothesize that delayed proportional feedback laws should be supported by the trials discussed in [GHKM06]. The delayed proportional feedback laws are given by

Figure 3.3: Regularized Inversion Algorithm

$$\begin{aligned}\hat{u}_p(t-\delta) &= -\left[\left(\dot{\mathbf{r}}\times\frac{\mathbf{r}}{|\mathbf{r}|}\right)\cdot\mathbf{z}_p\right]_{t-\delta}\\ \hat{v}_p(t-\delta) &= \left[\left(\dot{\mathbf{r}}\times\frac{\mathbf{r}}{|\mathbf{r}|}\right)\cdot\mathbf{y}_p\right]_{t-\delta}.\end{aligned}\tag{3.24}$$

3.4 Investigation of modified hypothesis

We propose a scheme for investigating the modified hypothesis in the following steps:

- Pick a trial, apply regularized inversion algorithm discussed in chapter 2 to extract true curvatures (u_p, v_p, u_e, v_e), speed signals $(\nu_p,\ \nu_e)$ and the associated frame information $[\mathbf{x}_p,\ \mathbf{y}_p,\ \mathbf{z}_p]$, $[\mathbf{x}_e,\ \mathbf{y}_e,\ \mathbf{z}_e]$, see figure (3.3).
- Using the above extracted information, the hypothesized curvatures $\hat{u}_p$, $\hat{v}_p$, $\hat{u}_e$, $\hat{v}_e$ can be obtained using the equations (3.24).

- Find a pair $\delta - \mu$ that

$$\min_{\mu \in \mathbb{R}} \left(\min_{\delta \in \mathbb{R}} \left(||u_p(t) - \mu \hat{u}_p(t-\delta)||^2 + ||v_p(t) - \mu \hat{v}_p(t-\delta)||^2 \right) \right) \tag{3.25}$$

- Since we hypothesize a linear relation between actual and hypothesized curvatures the above optimization may be effectively replaced by the alternative:

$$\min_{\mu \in \mathbb{R}} \left(||u_p(t) - \mu \hat{u}_p(t-\delta^*)||^2 + ||v_p(t) - \mu \hat{v}_p(t-\delta^*)||^2 \right) \tag{3.26}$$

  where δ^*:

$$\delta^* = \max_{\delta \in \mathbb{R}} \ \rho_{[\hat{u}_p(t-\delta) \ \ \hat{v}_p(t-\delta)] \ \ [u_p(t) \ \ v_p(t)]} \tag{3.27}$$

  and ρ is the statistical correlation defined as

$$\rho_{xy} = \frac{n \sum x_i y_i - \sum x_i \sum y_i}{\sqrt{n \sum x_i^2 - \left(\sum x_i \right)^2} \sqrt{n \sum y_i^2 - \left(\sum y_i \right)^2}} \tag{3.28}$$

- Construct a scatter plot of $[u_p(t), \ v_p(t)]$ vs $[\hat{u}_p(t-\delta^*), \hat{v}_p(t-\delta^*)]$ at δ^* `using the data of all the trials`

- If the underlying capture strategy is a delayed CATD, then the above choice of δ^* results in a linear fit with strong correlation.

3.5 Validation of the investigation process

The above investigation process needs to be validated. We generate trajectories for pursuer and evader using motion camouflage steering laws. Now assuming these trajectories as generated during bat- insect encounters, we apply the above investigation process. Since these trajectories are generated from a simulation, we have the freedom to set the delay, and we set δ^*=0. The scatter plot

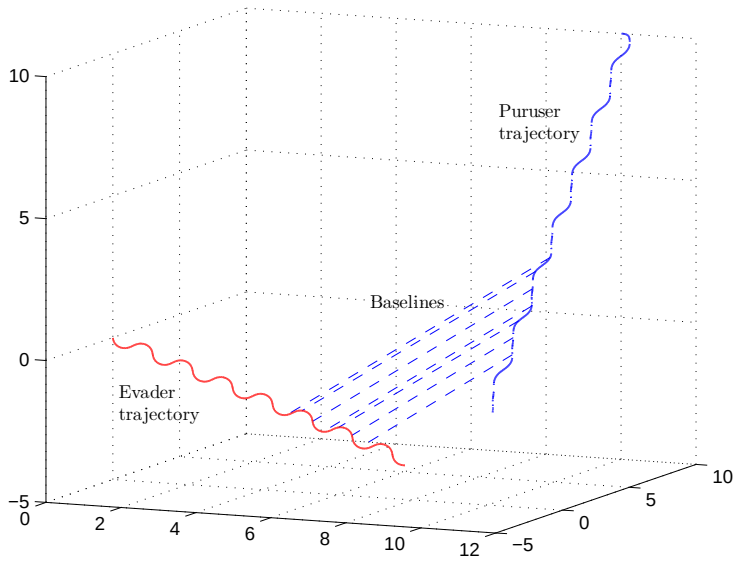

Figure 3.4: Pursuer evader trajectories generated by MC steering controls

$[u_p(t),\ v_p(t)]$ vs $[\hat{u}_p(t-\delta), \hat{v}_p(t-\delta)]$ at δ should be a linear fit with strong correlation at δ^*=0.

Figure (3.4) shows the trajectories of pursuit evasion model generated using motion camouflage steering laws, $u_e(t) = \sin(\frac{\pi}{2}t)$, $v_e(t) = \sin(\frac{\pi}{2}t)$, $\frac{\nu_e}{\nu_p} = 0.8$ and $\mu = 10$. Using the regularized inversion algorithm the actual curvatures u_p, v_p and other attributes are extracted. Then hypothesized curvatures $\hat{u}_p,\ \hat{v}_p$ are calculated using the equations (3.24).

Figure (3.5) shows the scatter plot $[u_p(t),\ v_p(t)]$ vs $[\hat{u}_p(t-\delta^*), \hat{v}_p(t-\delta^*)]$ at δ^*. Clearly the scatter plot is linear and has strong correlation $\rho = 0.9956$ at $\delta^* = 0$. Further, $\mu_{est} = 9.7844$ which is close to the actual $\mu = 10$. This study illustrates the investigation process.

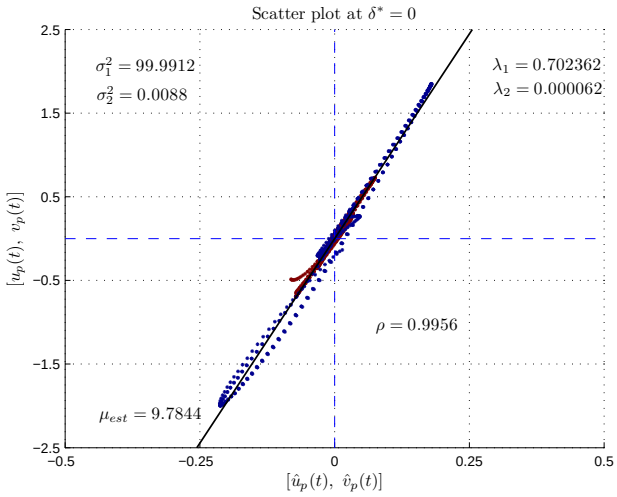

Figure 3.5: Result of correlation analysis with $\delta^* = 0$

3.6 Characterization of the ATTACK region

Eptesicus fuscus performs complex and rapid flight trajectories to catch insects in darkness. It produces directed ultrasound pulses and use the information contained in the returning echoes to detect, localize and track the prey. Based on the PPR (Pulse Production Rate) behavioral states of bat can be identified (refer [GM06]) as searching, approaching, tracking and attack. The PPR is low (5-10Hz) during the searching phase, once the bat senses the insect PPR increases to (20-50Hz) which is approach phase. During tracking phase PPR increases till 100Hz. In the attack phase, the PPR may be as high as 150-200 Hz terminating in insect pursuit and capture. This type of vocalization is referred to as terminal buzz. Figure (3.6) gives a demarcation of behavioral modes using vocalization data for a trial.

It is only during a portion of the trial, including the attack phase, can we expect

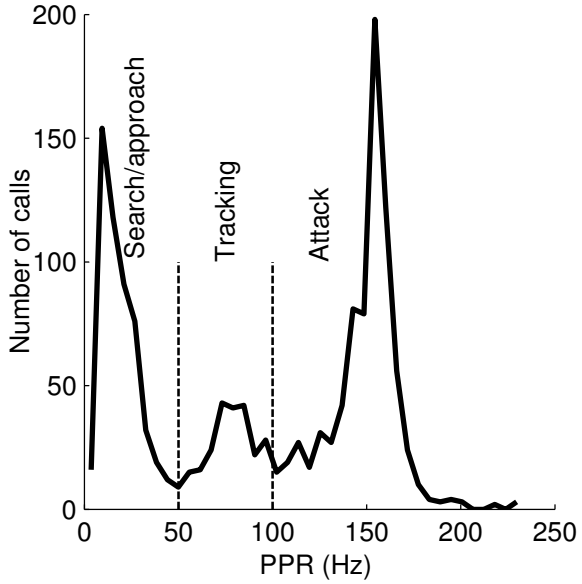

Figure 3.6: Demarcation of behaviorial modes of the bat based on vocalization data (reproduced from [GM06])

the baseline to be parallel in bat-insect trials. So, the trials need to be demarcated as in figure (3.6), and the flight paths only during these stages are considered for the investigation process. For the present study, we specify that the ATTACK region starts when the `ipi` (inter pulse interval) $= \left(\frac{1}{\text{PPR}}\right)$ drops below 10ms for the first time. Further, we specify that ATTACK region ends when the bat-insect separation falls below 5mm. Figure (3.7) shows the demarcation of ATTACK region based on the vocalization data for a sample trial.

3.7 Correlation analysis in the ATTACK region

Once the ATTACK region is identified, a correlation analysis is performed on the trials. The true curvatures $[u_p(t),\ v_p(t)]$ are stacked in a single vector using all the trials for t within the ATTACK region. Similarly for the hypothesized cur-

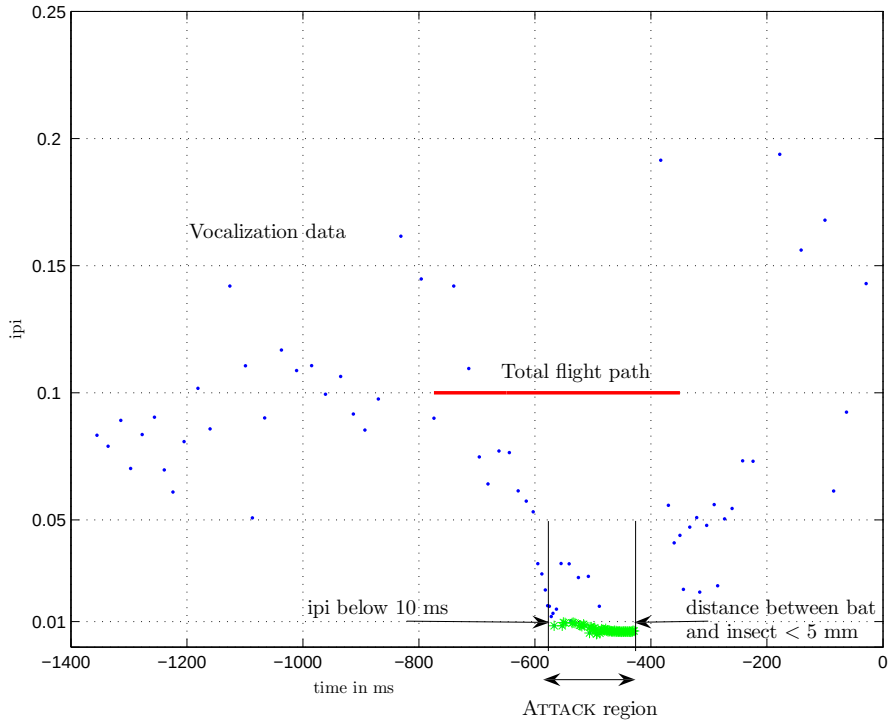

Figure 3.7: Characterization of ATTACK region

vatures $[\hat{u}_p(t-\delta),\ \hat{v}_p(t-\delta)]$ are assembled in a long vector. We seek to discover a possible linear relationship between the true curvature and the delayed hypothesized curvatures for same optimal delay δ^*. We calculate the correlation between two vectors, one representing true curvatures and another representing delayed hypothesized curvatures (constructed as above) using (3.28). Further, the delay, δ^*, corresponding to the maximum correlation is calculated using (3.27).

3.8 Results with bat-insect trials

We considered 18 successful trials (bat eventually catches the insect) for the statistical validation study. The bat-insect trajectories were reconstructed using

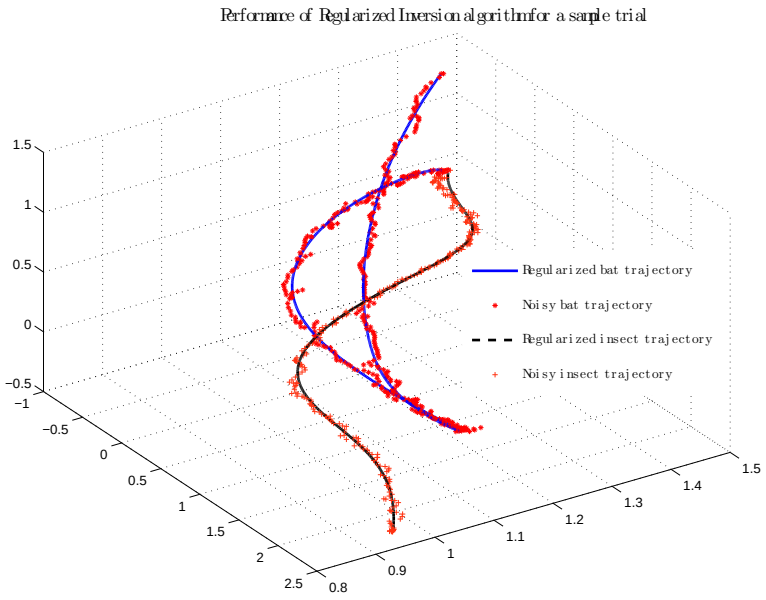

Figure 3.8: Performance of the regularized inversion algorithm for a sample trial

Trial	Fitting Error $=\frac{1}{N}\sum_{i=1}^{N}\|\|\gamma_i - \gamma(iM)\|\|^2$
1	3.827001e-04
2	4.391072e-04
3	5.217596e-04
4	2.892920e-04
5	2.623724e-04
6	5.448956e-04
7	4.579816e-04
8	4.221725e-06
9	1.008097e-04
10	6.310765e-04
11	2.476038e-05
12	5.044202e-05
13	3.861575e-05
14	7.523885e-05
15	5.924500e-04
16	4.222170e-05
17	1.270047e-05
18	6.509249e-04

Table 3.1: Performance of regularized inversion algorithm on the trials

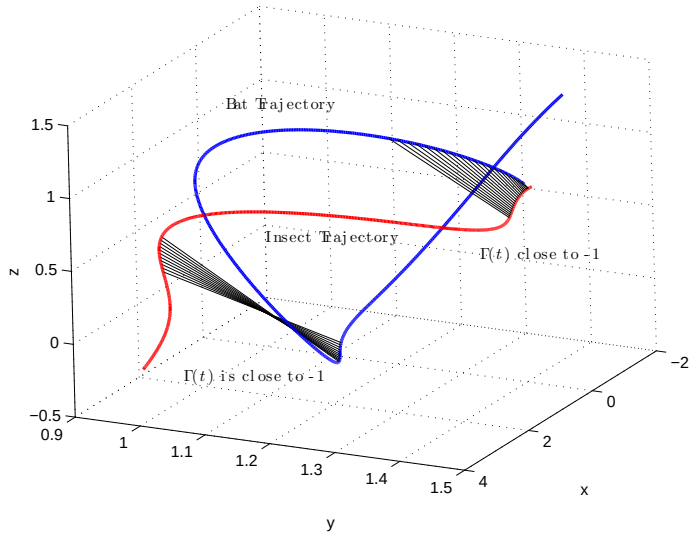

Figure 3.9: Bat - insect trial, baseline is parallel before the capture

the images from two high speed video cameras ([GHKM06]). The frame rate of the cameras is 250Hz, so the bat-insect data consists of trajectories sampled at 4ms intervals. As the regularized inversion algorithm is sub frame adaptable, we reconstruct the trajectory with 2ms intervals. The reconstruction resolution can be improved further but it is computationally expensive.

During reconstruction, we first choose the regularization parameter λ to be very small. This choice of λ results in a small fitting error. In order to achieve smooth curvatures we increase λ in small steps. We observe that, for smooth trajectories a small change in λ does not affect the fitting error, whereas, a small change in λ does affect the fitting error for noisy trajectories. We choose to increase λ to obtain smooth curvatures, the regularization parameter is taken as $\lambda = 0.01$ for noisy trials and $\lambda = 0.005$ for smooth trials.

Figure (3.8) shows the performance of regularized inversion method on a single

trial, where the trajectory has been reconstructed using the inputs. This clearly shows the advantage of using regularized inversion algorithm when the data is noisy. Table (3.1) summarizes the algorithm performance on all the trials in terms of reconstruction error.

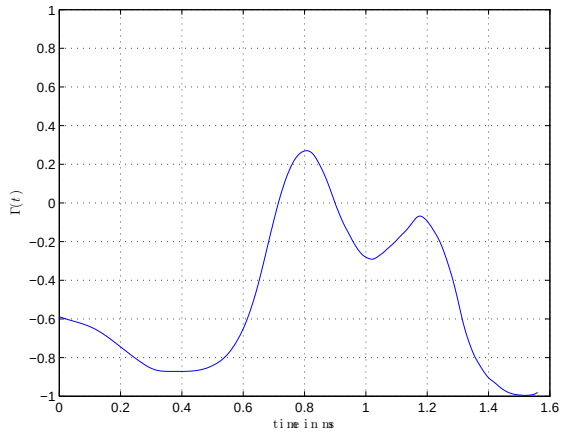

Figure 3.10: $\Gamma(t)$ is close to -1 when the bat initially approaches the insect, then rises above 0 when the bat misses the insect and eventually goes to -1 near capture.

Figure (3.9) shows the flight path of a bat - insect trial, it is clearly seen that near the attack/capture region base line remains parallel (visually). We calculate $\Gamma(t)$, a measure of distance from motion camouflage manifold, to cross check our hypothesis. For this trial, first the bat approaches the insect, misses it, eventually capturing the insect. The $\Gamma(t)$ plot of this trial is given in figure (3.10), clearly there is a dip corresponding to the initial approach and the final dip (close to -1) corresponds to capture. This behavior with $\Gamma(t)$ is consistent among all the successful trials.

Figure (3.11) shows the plots of true curvatures ($u_p(t)$, $v_p(t)$) and hypothesized curvatures ($\hat{u}_p(t)$, $\hat{v}_p(t)$) for trials #1 and #3 respectively. The hypothesized curva-

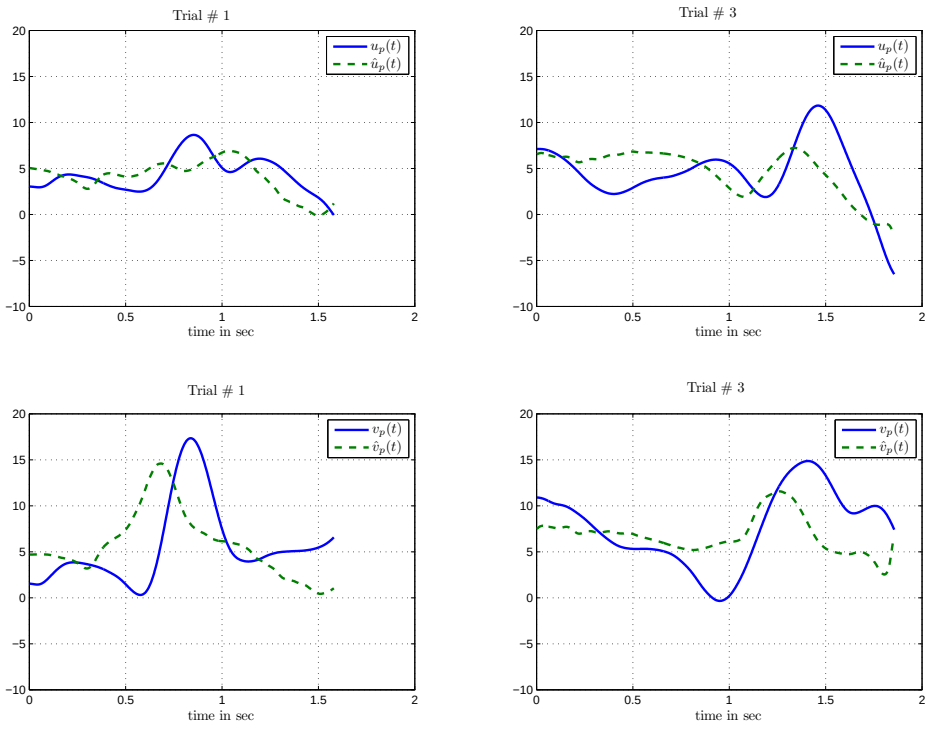

Figure 3.11: Curvature profiles for the Trials #1 and #3 : The hypothesized curvatures ($\hat{u}_p,\ \hat{v}_p$) resemble shifted and scaled versions of true curvatures ($u_p,\ v_p$).

ture resembles a scaled and shifted version of the true curvature, shifting according to the delay δ^*, and scaling corresponds to the gain μ. Now, we evaluate statistically relevant values of δ^* and μ using all the trials.

First, a vector corresponding to true curvatures is obtained by stacking true curvatures from the corresponding ATTACK regions of all the 18 trials. Then, another vector corresponding to δ shifted hypothesized curvatures is obtained.

We estimate three quantities, $\rho_{u_p(t)\hat{u}_p(t)}$, $\rho_{v_p(t)\hat{v}_p(t)}$ and $\rho_{[u_p(t),\ v_p(t)]\ [\hat{u}_p(t),\hat{v}_p(t)]}$ as a function of δ using all the trials. Figures (3.12), (3.13) and (3.14) show the variation of correlations with δ. Peaks were observed at 96ms, 136ms and 112ms. Since we are interested in combined effect of both the curvatures, we choose $\delta^* = 112ms$.

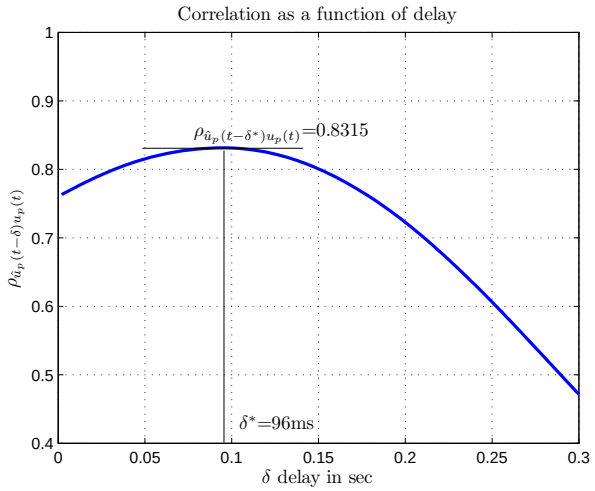

Figure 3.12: Correlation as a function of δ with the curvatures $u_p(t)$ and $\hat{u}_p(t)$

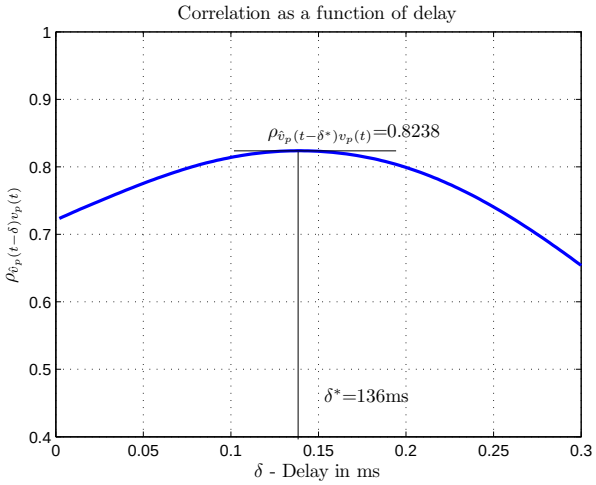

Figure 3.13: Correlation as a function of δ with the curvatures $v_p(t)$ and $\hat{v}_p(t)$

We think this corresponds to the combined effect of sensory motor processing and acoustic delay (See related remarks in [GHKM06]). Figures (3.15), (3.16) and (3.17) refer to the scatter plots of true and hypothesized curvatures at a delay (δ^*) value where the corresponding correlations are maximum. Visually, we notice that data is directly suggesting a linear relation between the curvatures $u_p(t)$ and $\hat{u}_p(t-\delta^*)$, $v_p(t)$ and $\hat{v}_p(t-\delta^*)$ at δ^*. Upon doing a principal component analysis on the data we observe that the data is directional as variance of one component is very high

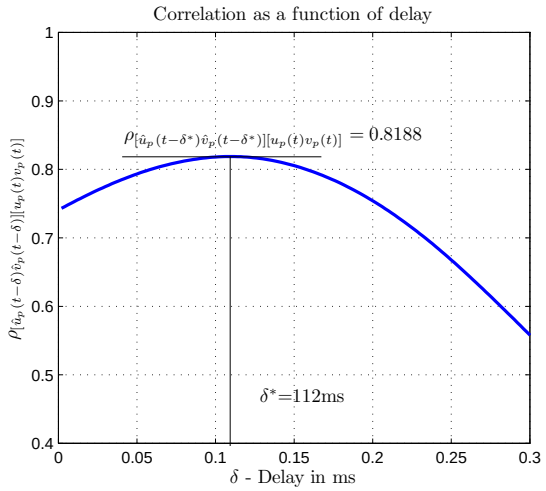

Figure 3.14: Correlation as a function of δ with the curvatures $[u_p(t),\ v_p(t)]$ and $[\hat{u}_p(t),\ \hat{v}_p(t)]$

.

(refer table (3.2)). Further, we observe a correlation exceeding 0.8 between true and hypothesized curvatures (using both u_p, v_p) at δ^*= 112ms, which gives an estimate of the gain as $\mu_{est} = 0.48065$. Thus, 112 ms corresponds to the delay associated with sensory motor processing and acoustic delay. During the attack phase the acoustic delay is nearly 10ms (see [GHKM06]), so the delay contribution from sensory motor processing is nearly 100 ms.

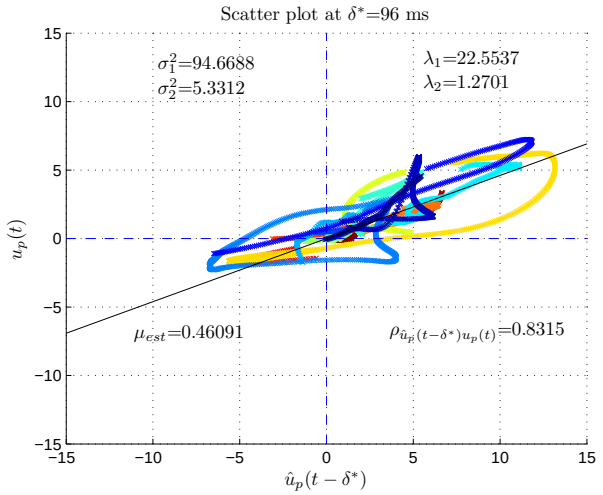

Figure 3.15: Scatter plot of $\hat{u}_p(t-\delta^*)$ vs $u_p(t)$, with δ^*=96ms

	$\hat{u}_p - u_p$	$\hat{v}_p - v_p$	$[\hat{u}_p\ \hat{v}_p] - [u_p\ v_p]$
δ^*	96ms	136ms	112ms
λ_1	22.5537	22.9764	22.6134
λ_2	1.2701	1.728	1.5442
σ_1^2	94.6688	93.0052	93.608
σ_2^2	5.3312	6.9948	6.392
μ_{est}	0.46091	0.50922	0.48065
ρ	0.8315	0.8238	0.8188

Table 3.2: Summary of the statistical evaluation of motion camouflage control laws. λ_1 and λ_2 represent the principal component variances, i.e., eigenvalues of the covariance matrix (constructed with $[\hat{u}_p\ \hat{v}_p]$ and $[u_p\ v_p]$ at optimal delays). σ_1^2 and σ_2^2 represent the percentage of total variance explained by principle components.

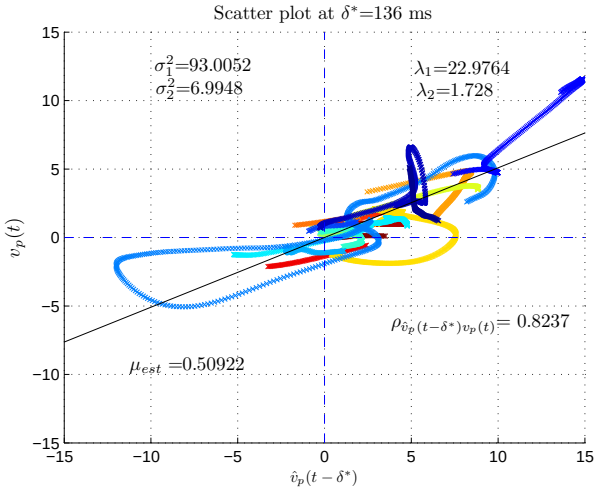

Figure 3.16: Scatter plot of $\hat{v}_p(t-\delta^*)$ vs $v_p(t)$, with δ^*=136ms

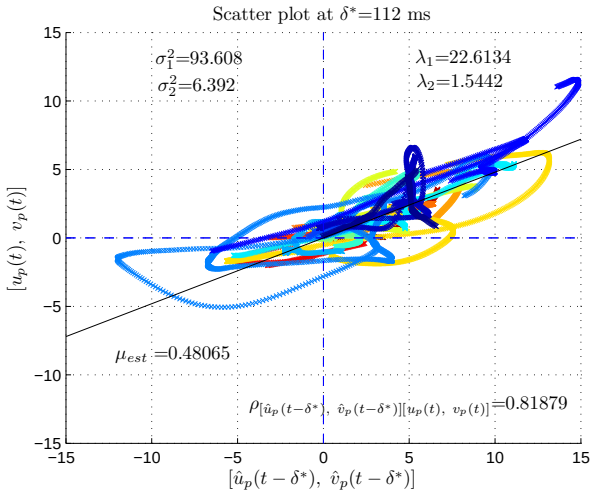

Figure 3.17: Scatter plot of $[\hat{u}_p(t-\delta^*),\ \hat{v}_p(t-\delta^*)]$ vs $[u_p(t),\ v_p(t)]$, with δ^*=112ms

Chapter 4

Delays in Motion Camouflage Steering Laws

4.1 Introduction

In chapter 1 we introduced a type of stealthy pursuit behavior called motion camouflage. Feedback laws that drive the system to a state of motion camouflage have been derived for planar and 3D geometries. Further, the only free parameter in these feedback laws is the feedback gain μ. In the absence of delays (due to sensorimotor processing and communication) it has been shown in [JK06, RJK06] that the higher the value of feedback gain, the more effectively the system is driven close to a state of motion camouflage. However, in a practical setting, the delays due to sensing and sensorimotor processing are inevitable and this would limit the value of gain μ. In a recent study [GHKM06], using experimental data, the values of sensorimotor delay and gain were estimated for bat-insect engagements. In this chapter we investigate, analytically, the effect of delay on pertinent values of gain, and plausibility of reaching a state of motion camouflage. We limit our investigation to the planar case. However, an extension to the 3D case is straightforward.

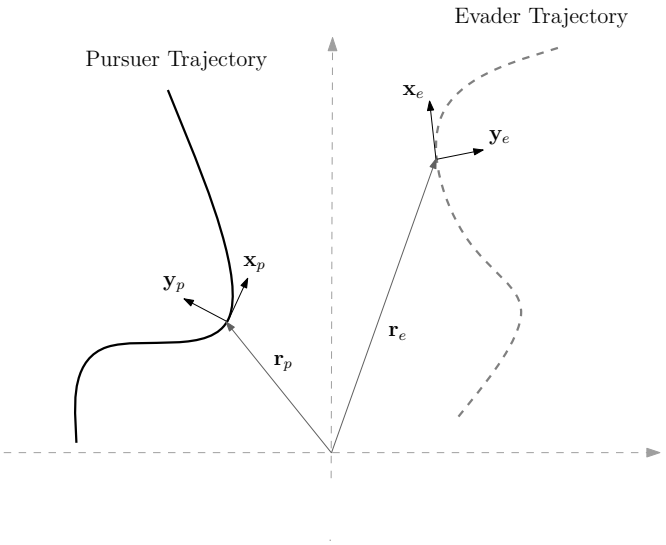

Figure 4.1: Planar pursuit engagement modeled using natural Frenet frames.

4.2 Delays in motion camouflage - Planar case

Feedback laws that drive a pursuer evader system to a state of motion camouflage in finite time are discussed for the delay free case (refer [JK06, RJK06]). A model of the pursuit evasion system, as shown in figure (4.1) is given by the equations.

$$\begin{aligned}
\dot{\mathbf{r}}_p &= \mathbf{x}_p, \\
\dot{\mathbf{x}}_p &= u_p \mathbf{y}_p, \\
\dot{\mathbf{y}}_p &= -u_p \mathbf{x}_p, \qquad (4.1) \\
\dot{\mathbf{r}}_e &= \nu \mathbf{x}_e, \\
\dot{\mathbf{x}}_e &= \nu u_e \mathbf{y}_e, \\
\dot{\mathbf{y}}_e &= -\nu u_e \mathbf{x}_e, \qquad (4.2)
\end{aligned}$$

The steering control of the evader, u_e, is prescribed. In [JK06] the authors analyze the feedback laws for motion camouflage that takes the form

$$u_p = -\mu \left(\frac{\mathbf{r}}{|\mathbf{r}|} \cdot \dot{\mathbf{r}}^{\perp} \right), \tag{4.3}$$

where, the "baseline vector", $\mathbf{r} = \mathbf{r}_p - \mathbf{r}_e$ is the relative position of the pursuer with respect to the evader. $\mu > 0$ is the feedback gain parameter [JK06]. We assume $0 < \nu < 1$, so that the pursuer moves faster than the evader. By incorporating delay, due to communication/sensorimotor processing, $u_p(t)$ in the equation (4.1) is replaced by $u_p(t - \tau)$,

$$\begin{aligned} \dot{\mathbf{r}}_p(t) &= \mathbf{x}_p(t), \\ \dot{\mathbf{x}}_p(t) &= u_p(t-\tau)\mathbf{y}_p(t), \\ \dot{\mathbf{y}}_p(t) &= -u_p(t-\tau)\mathbf{x}_p(t). \end{aligned} \tag{4.4}$$

In what follows we assume that the evader cannot make arbitrary sharp turns, $|u_e(t)| \leq u_{max}$.

4.2.1 Distance from a state of motion camouflage

From [JK06], we let

$$\Gamma = \frac{\mathbf{r}}{|\mathbf{r}|} \cdot \frac{\dot{\mathbf{r}}}{|\dot{\mathbf{r}}|} \tag{4.5}$$

Γ is well defined if $|\mathbf{r}| \neq 0$, since

$$|\dot{\mathbf{r}}| = |\dot{\mathbf{r}}_p - \dot{\mathbf{r}}_e| = |\mathbf{x}_p - \nu \mathbf{x}_e| \geq 1 - \nu > 0. \tag{4.6}$$

In that case, $-1 \leq \Gamma \leq 1$. It follows that

$$\Gamma^2 = 1 - \frac{|\mathbf{w}|^2}{|\dot{\mathbf{r}}|^2} \tag{4.7}$$

Since (in chapter 3), $\mathbf{w} \equiv 0$ on an interval is a necessary and sufficient condition for motion camouflage w.r.t. infinity, it follows that Γ^2 is a measure of deviation from a state of motion camouflage. Now, $\Gamma(t) \to -1(+1)$, then the pursuer evader system is approaching motion camouflage while reducing the separation (increasing the separation).

In what follows we will develop bounds for various quantities when $|\mathbf{r}| > r_0 > 0$ where we will choose r_0 to be sufficiently small.

Differentiating Γ along the trajectories of (4.2) and (4.4) gives:

$$\begin{aligned} \dot{\Gamma} &= \left(\frac{\dot{\mathbf{r}} \cdot \dot{\mathbf{r}} + \mathbf{r} \cdot \ddot{\mathbf{r}}}{|\mathbf{r}||\dot{\mathbf{r}}|} \right) - \left(\frac{\mathbf{r} \cdot \dot{\mathbf{r}}}{|\dot{\mathbf{r}}|} \right) \left(\frac{\mathbf{r} \cdot \dot{\mathbf{r}}}{|\mathbf{r}|^3} \right) - \left(\frac{\mathbf{r} \cdot \dot{\mathbf{r}}}{|\mathbf{r}|} \right) \left(\frac{\dot{\mathbf{r}} \cdot \ddot{\mathbf{r}}}{|\dot{\mathbf{r}}|^3} \right) \\ &= \frac{|\dot{\mathbf{r}}|}{|\mathbf{r}|} \left(1 - \Gamma^2\right) + \frac{1}{|\dot{\mathbf{r}}|} \left[\frac{\mathbf{r}}{|\mathbf{r}|} - \left(\frac{\mathbf{r}}{|\mathbf{r}|} \cdot \frac{\dot{\mathbf{r}}}{|\dot{\mathbf{r}}|} \right) \frac{\dot{\mathbf{r}}}{|\dot{\mathbf{r}}|} \right] \cdot \ddot{\mathbf{r}} \end{aligned} \tag{4.8}$$

Now,

$$\left[\frac{\mathbf{r}}{|\mathbf{r}|} - \left(\frac{\mathbf{r}}{|\mathbf{r}|} \cdot \frac{\dot{\mathbf{r}}}{|\dot{\mathbf{r}}|}\right)\frac{\dot{\mathbf{r}}}{|\dot{\mathbf{r}}|}\right] \;=\; \left(\frac{\mathbf{r}}{|\mathbf{r}|} \cdot \dot{\mathbf{r}}^{\perp}\right)\frac{\dot{\mathbf{r}}^{\perp}}{|\dot{\mathbf{r}}|^2}$$

Define w as

$$w = -\left(\frac{\mathbf{r}}{|\mathbf{r}|} \cdot \dot{\mathbf{r}}^{\perp}\right). \tag{4.9}$$

Then $u_p(t) = \mu w$ and (4.8) becomes

$$\dot{\Gamma} = \frac{|\dot{\mathbf{r}}|}{|\mathbf{r}|}\left(1 - \Gamma^2\right) - \frac{w}{|\dot{\mathbf{r}}|^3}\dot{\mathbf{r}}^{\perp} \cdot \ddot{\mathbf{r}} \tag{4.10}$$

We know,

$$\dot{\mathbf{r}} = \mathbf{x}_p - \nu\mathbf{x}_e. \tag{4.11}$$

So,

$$\dot{\mathbf{r}}^{\perp} = \mathbf{y}_p - \nu\mathbf{y}_e, \tag{4.12}$$

and

$$\ddot{\mathbf{r}} = u_p(t-\tau)\mathbf{y}_p - \nu^2 u_e\mathbf{y}_e, \tag{4.13}$$

which using the above two expressions gives,

$$\dot{\mathbf{r}}^{\perp} \cdot \ddot{\mathbf{r}} = \left[1 - \nu\left(\mathbf{y}_p \cdot \mathbf{y}_e\right)\right] u_p(t-\tau) + \nu^2\left[\nu - \left(\mathbf{y}_p \cdot \mathbf{y}_e\right)\right] u_e. \tag{4.14}$$

Now, (4.10) can be written as :

$$\dot{\Gamma} = \frac{|\dot{\mathbf{r}}|}{|\mathbf{r}|}\left(1-\Gamma^2\right) - \frac{w}{|\dot{\mathbf{r}}|^3}\left[1-\nu\left(\mathbf{y}_p\cdot\mathbf{y}_e\right)\right]u_p(t-\tau) - \frac{w}{|\dot{\mathbf{r}}|^3}\nu^2\left[\nu-\left(\mathbf{y}_p\cdot\mathbf{y}_e\right)\right]u_e \quad (4.15)$$

We investigate the effect of delay τ on $\dot{\Gamma}(t)$ and the plausibility of reaching a state of motion camouflage. It has been pointed that in delay differential equations such as (4.4), if one were to use Taylor series approximations to represent solutions, then the resulting errors would grow without bound [MT74]. Here we take an alternative approach, with out approximations, based on the scalar mean value theorem. Since $u_p(t)$ is a continuous function, from mean value theorem there exists $t^* \in [t-\tau, t]$ such that

$$\dot{u}_p(t^*) = \frac{u_p(t) - u_p(t-\tau)}{\tau}. \quad (4.16)$$

Clearly,

$$u_p(t-\tau) = u_p(t) - \tau\dot{u}_p(t^*) = u_p(t) - \mu\tau\dot{w}(t^*). \quad (4.17)$$

Now,

$$\begin{aligned}
\dot{w}(t^*) &= -\left[\frac{d}{dt}\left(\frac{\mathbf{r}}{|\mathbf{r}|}\right)\cdot\dot{\mathbf{r}}^{\perp} + \left(\frac{\mathbf{r}}{|\mathbf{r}|}\right)\cdot\left(\ddot{\mathbf{r}}^{\perp}\right)\right]\Big|_{t=t^*} \\
&= -\left[\frac{1}{|\mathbf{r}|}\left(\dot{\mathbf{r}} - \left(\frac{\mathbf{r}}{|\mathbf{r}|}\cdot\dot{\mathbf{r}}\right)\frac{\mathbf{r}}{|\mathbf{r}|}\right)\cdot\dot{\mathbf{r}}^{\perp} + \left(\frac{\mathbf{r}}{|\mathbf{r}|}\right)\cdot\left(\ddot{\mathbf{r}}^{\perp}\right)\right]\Big|_{t=t^*} \\
&= \frac{1}{|\mathbf{r}|}\left(\frac{\mathbf{r}}{|\mathbf{r}|}\cdot\dot{\mathbf{r}}\right)\left(\frac{\mathbf{r}}{|\mathbf{r}|}\cdot\dot{\mathbf{r}}^{\perp}\right) - \left(\frac{\mathbf{r}}{|\mathbf{r}|}\right)\cdot\left(\ddot{\mathbf{r}}^{\perp}\right)\Big|_{t=t^*}
\end{aligned} \quad (4.18)$$

and we write,

$$\frac{\mathbf{r}}{|\mathbf{r}|}\cdot\ddot{\mathbf{r}}^{\perp} = u_p(t-\tau)\left(\frac{\mathbf{r}}{|\mathbf{r}|}\cdot\mathbf{x}_p\right) - \nu^2 u_e\left(\frac{\mathbf{r}}{|\mathbf{r}|}\cdot\mathbf{x}_e\right) \tag{4.19}$$

From (4.11)

$$1-\nu \le |\dot{\mathbf{r}}| = |\dot{\mathbf{r}}^{\perp}| \le 1+\nu \tag{4.20}$$

Hence,

$$|u_p(t)| \le \mu(1+\nu) \quad \forall\ t. \tag{4.21}$$

Using the above equations $\dot{w}(t^*)$ is bounded as:

$$|\dot{w}| \le \frac{(1+\nu)^2}{2\ |\mathbf{r}|} + \mu(1+\nu) + \nu^2 u_{max} \tag{4.22}$$

From (4.15) and (4.16)

$$\begin{aligned}
\dot{\Gamma} &= \frac{|\dot{\mathbf{r}}|}{|\mathbf{r}|}\left(1-\Gamma^2\right) - \frac{w}{|\dot{\mathbf{r}}|^3}\left[1-\nu\left(\mathbf{y}_p\cdot\mathbf{y}_e\right)\right]u_p(t) - \frac{w}{|\dot{\mathbf{r}}|^3}\nu^2\left[\nu-\left(\mathbf{y}_p\cdot\mathbf{y}_e\right)\right]u_e \\
&\quad +\mu\tau\dot{w}(t^*)\frac{w}{|\dot{\mathbf{r}}|^3}\left[1-\nu\left(\mathbf{y}_p\cdot\mathbf{y}_e\right)\right] \\
&= \frac{|\dot{\mathbf{r}}|}{|\mathbf{r}|}\left(1-\Gamma^2\right) - \frac{\mu}{|\dot{\mathbf{r}}|}\left[1-\nu\left(\mathbf{y}_p\cdot\mathbf{y}_e\right)\right]\left(1-\Gamma^2\right) - \frac{w}{|\dot{\mathbf{r}}|^3}\nu^2\left[\nu-\left(\mathbf{y}_p\cdot\mathbf{y}_e\right)\right]u_e \\
&\quad +\mu\tau\dot{w}(t^*)\frac{w}{|\dot{\mathbf{r}}|^3}\left[1-\nu\left(\mathbf{y}_p\cdot\mathbf{y}_e\right)\right] \\
&\le -\left(1-\Gamma^2\right)\left(\frac{\mu}{|\dot{\mathbf{r}}|}\left[1-\nu\left(\mathbf{y}_p\cdot\mathbf{y}_e\right)\right] - \frac{|\dot{\mathbf{r}}|}{|\mathbf{r}|}\right) + \sqrt{1-\Gamma^2}\ \frac{\nu^2(1+\nu)u_{max}}{(1-\nu)^2} \\
&\quad +\mu\tau\ \sqrt{1-\Gamma^2}\ \frac{(1+\nu)}{(1-\nu)^2}\ \left(\frac{(1+\nu)^2}{2\ |\mathbf{r}|} + \mu(1+\nu) + \nu^2 u_{max}\right)
\end{aligned}$$

$$
\begin{aligned}
&\leq -\left(1-\Gamma^2\right)\left(\mu\,\frac{1-\nu}{1+\nu}-\frac{1+\nu}{|\mathbf{r}|}\right)+\sqrt{1-\Gamma^2}\,\frac{\nu^2(1+\nu)u_{max}}{(1-\nu)^2}\\
&\quad +\mu\tau\,\sqrt{1-\Gamma^2}\,\frac{(1+\nu)}{(1-\nu)^2}\,\left(\frac{(1+\nu)^2}{2\,|\mathbf{r}|}+\mu(1+\nu)+\nu^2u_{max}\right)\\
&\leq -\left(1-\Gamma^2\right)\left(\mu\,\frac{1-\nu}{1+\nu}-\frac{1+\nu}{r_0}\right)+\sqrt{1-\Gamma^2}\,\frac{\nu^2(1+\nu)u_{max}}{(1-\nu)^2}\\
&\quad +\mu\tau\,\sqrt{1-\Gamma^2}\,\frac{(1+\nu)}{(1-\nu)^2}\,\left(\frac{(1+\nu)^2}{2\,r_0}+\mu(1+\nu)+\nu^2u_{max}\right). \qquad (4.23)
\end{aligned}
$$

Letting

$$
c_0=\mu\left(\frac{1-\nu}{1+\nu}\right)-\frac{1+\nu}{r_0} \qquad (4.24)
$$

and

$$
c_1=\frac{\nu^2(1+\nu)u_{max}}{(1-\nu)^2}, \qquad (4.25)
$$

inequality (4.23) can be written as

$$
\dot{\Gamma}\;\leq\;-c_0(1-\Gamma^2)+\sqrt{1-\Gamma^2}\left[c_1+\mu\tau\left(c_1+\left(\frac{1+\nu}{1-\nu}\right)^2\left(\mu+\frac{1+\nu}{2\,r_0}\right)\right)\right], \qquad (4.26)
$$

for $|\mathbf{r}|>r_0$, where c_0 depends on μ. Further, we require $c_0>0$ for the term $-(1-\Gamma)^2c_0$ to be negative. This condition gives a lower bound on μ as

$$
\mu>\frac{(1+\nu)^2}{(1-\nu)r_0}. \qquad (4.27)
$$

With $\tau=0$, the above inequality identical to inequality (3.6) in [JK06]. Suppose that we are given $0<\epsilon\ll 1$, and if $c_0>\frac{1}{\sqrt{\epsilon}}\left[c_1+\mu\tau\left(c_1+\left(\frac{1+\nu}{1-\nu}\right)^2\left(\mu+\frac{1+\nu}{2\,r_0}\right)\right)\right]$,

then for $|\mathbf{r}| > r_0$ and $1 - \Gamma^2 > \epsilon$ we have,

$$\dot{\Gamma} \;\leq\; -(1-\Gamma^2)c_2 \tag{4.28}$$

where

$$c_2 = \left(c_0 - \frac{1}{\sqrt{\epsilon}} \left[c_1 + \mu\tau \left(c_1 + \left(\frac{1+\nu}{1-\nu} \right)^2 \left(\mu + \frac{1+\nu}{2\ r_0} \right) \right) \right] \right) > 0. \tag{4.29}$$

From inequality (4.28) we write

$$\frac{d\Gamma}{1-\Gamma^2} \leq -c_2 dt$$

integrating both sides, we have

$$\int_{\Gamma_0}^{\Gamma} \frac{d\tilde{\Gamma}}{1-\tilde{\Gamma}^2} \leq -\int_0^t c_2 d\tau = -c_2 t \tag{4.30}$$

with $\Gamma_0 = \tilde{\Gamma}_{|_{t=0}}$,

$$\int_{\Gamma_0}^{\Gamma} \frac{d\tilde{\Gamma}}{1-\tilde{\Gamma}^2} = \tanh^{-1}(\Gamma(t)) - \tanh^{-1}(\Gamma_0) \leq -c_2 t. \tag{4.31}$$

We know $\Gamma = \frac{\mathbf{r}}{|\mathbf{r}|} \cdot \frac{\dot{\mathbf{r}}}{|\dot{\mathbf{r}}|}$, so

$$\frac{d}{dt}|\mathbf{r}| = |\Gamma(t)||\dot{\mathbf{r}}| \geq -(1+\nu). \tag{4.32}$$

From (4.30), we conclude that

$$|\mathbf{r}(t)| \geq |\mathbf{r}(0)| - (1+\nu)t, \ \forall t > 0, \tag{4.33}$$

further,

$$|\mathbf{r}(t)| \geq r_0, \ \forall t \leq \frac{|\mathbf{r}(0|) - r_0}{1+\nu} \tag{4.34}$$

We assume, $|\mathbf{r}(0)| > r_0$, then defining

$$T = \frac{|\mathbf{r}(0)| - r_0}{1+\nu} > 0 \tag{4.35}$$

to be a lower bound on the interval of time over which we can guarantee that $\dot{\Gamma} \leq 0$, we conclude that

$$\Gamma(T) \leq \tanh\left(\tanh^{-1}\Gamma_0 - c_2 T\right). \tag{4.36}$$

Since, $\dot{\Gamma} \leq -c_2\epsilon$, $\Gamma(T)$ can be driven below $-1+\epsilon$ by choosing a sufficiently large c_2. So, we seek to drive $\Gamma(t_1) \leq -1+\epsilon$ for $t_1 \in (0, T]$. From (4.36), we have

$$\begin{aligned}
\tanh\left(\tanh^{-1}(\Gamma_0) - c_2 T\right) &\leq -1+\epsilon \\
c_2 &\geq \frac{(1+\nu)\left(\tanh^{-1}(\Gamma_0) - \frac{1}{2}\ln\left(\frac{\epsilon}{2-\epsilon}\right)\right)}{|\mathbf{r}(0)| - r_0} \\
&= \frac{(1+\nu)\left[\frac{1}{2}\ln\left(\frac{1+\Gamma_0}{1-\Gamma_0}\ \frac{2-\epsilon}{\epsilon}\right)\right]}{|\mathbf{r}(0)| - r_0}
\end{aligned}$$

$$c_0 - \frac{1}{\sqrt{\epsilon}}\left[c_1 + \mu\tau\left(c_1 + \left(\frac{1+\nu}{1-\nu}\right)^2\left(\mu + \frac{1+\nu}{2\ r_0}\right)\right)\right] \ \geq \ \frac{(1+\nu)\left[\frac{1}{2}\ln\left(\frac{1+\Gamma_0}{1-\Gamma_0}\ \frac{2-\epsilon}{\epsilon}\right)\right]}{|\mathbf{r}(0)| - r_0} \tag{4.37}$$

The right hand side of the above inequality is a monotone decreasing function of ϵ and negative for $\epsilon > 1 + \Gamma_0$. To ensure the condition (4.29) we define

$$\delta(\epsilon) = \max\left\{0, \frac{(1+\nu)\left[\frac{1}{2}\ln\left(\frac{1+\Gamma_0}{1-\Gamma_0}\ \frac{2-\epsilon}{\epsilon}\right)\right]}{|\mathbf{r}(0)| - r_0}\right\} \tag{4.38}$$

So, the quadratic (in μ not in ϵ) inequality (4.37) is clearly written as:

$$\left[\mu\left(\frac{1-\nu}{1+\nu}\right) - \left(\frac{1+\nu}{r_0} + \frac{c_1}{\sqrt{\epsilon}}\right)\right] - \frac{\tau}{\sqrt{\epsilon}}\mu\left[c_1 + \left(\frac{1+\nu}{1-\nu}\right)^2\left(\mu + \frac{1+\nu}{2\ r_0}\right)\right] \geq \delta(\epsilon) \tag{4.39}$$

Given τ and ϵ, we seek to find a feasible set of μ that satisfies the above inequality, i.e., pertinent values of gain that drive the system to a state of motion camouflage at some finite time $t_1 \leq T$. We discuss this in detail in section (4.2.3). Assuming such a gain μ exists one can give a result on teachability of motion camouflage.

4.2.2 Statement of result

We give sufficient conditions to drive the system defined by (4.2) and (4.4) very close to a state of motion camouflage in finite time as :

Proposition 4.2.1 *Consider the system (4.2) with (4.4) and control law (4.3) subject to a time delay $\tau > 0$, $0 < \epsilon << 1$, and the following hypotheses:*

(A1) $0 < \nu < 1$ *(and* ν *is constant),*

(A2) u_e *is continuous and* $|u_e|$ *is bounded,*

(A3) $\Gamma_0 = \Gamma(0) < 1 - \epsilon$*, and*

(A4) $|\mathbf{r}(0)| > 0$.

Let $0 < r_0 < |\mathbf{r}(0)|$*, and* $T = \frac{|\mathbf{r}(0)| - r_0}{1+\nu}$

$$\delta = \max\left(0, \frac{1}{2}\left(\frac{1+\nu}{|\mathbf{r}(0)| - r_0}\right)\ln\left[\left(\frac{1+\Gamma_0}{1-\Gamma_0}\right)\left(\frac{2-\epsilon}{\epsilon}\right)\right]\right). \tag{4.40}$$

Then there exists a finite time t_1 *for which* $\Gamma(t_1) \leq -1 + \epsilon$ *(i.e., motion camouflage is accessible in finite time), provided there exists a value of* $\mu > 0$ *which satisfies (4.27) and*

$$\begin{aligned} c_2 &= c_0 - \frac{1}{\sqrt{\epsilon}}\left[c_1 + \tau\mu\left(c_1 + \left(\frac{1+\nu}{1-\nu}\right)^2\left(\mu + \frac{1+\nu}{2r_0}\right)\right)\right] \\ &> \delta, \end{aligned} \tag{4.41}$$

where c_0 *and* c_1 *are given by (4.24) and (4.25) respectively.*

Proof: Choose $r_0 > 0$ such that $\mathbf{r}(0) > r_0$. For a given $\tau > 0$ and $0 < \epsilon \ll 1$, choose a sufficiently large c_0 to ensure that (4.40) holds and bounds on μ given by (4.25) and (4.38) are also satisfied. Then for a choice of μ with in these bounds, we are guaranteed to achieve $\Gamma(t_1) \leq -1 + \epsilon$ at some finite time $t_1 \leq T$. □

Remarks:

- For $\tau = 0$ Proposition (3.3) in [JK06] guarantees the existence of (a range of) values of μ which meet the hypothesis above that $c_2 > \delta$, for any choice of

$\epsilon > 0$, $0 < \nu < 1$, $|\mathbf{r}(0)| > 0$ and $\Gamma_0 < 1$. Since c_2 is linear in τ, (holding μ fixed), it follows that for small values of τ the in equality $c_2 > \delta$ remains true, and the conclusion of the above proposition are true. Below we examine in greater detail the role of τ on admissible μ.

- By taking $|\mathbf{r}(0)|$ arbitrarily large, δ may be made arbitrarily close to zero. Intuitively, this means that a large initial separation facilitates reaching a motion camouflage state. Corresponding remarks can be made about the effects of Γ_0 and ϵ on δ, as well.

4.2.3 Interpretation of $c_2(\mu, \tau, \epsilon) > \delta(\epsilon)$ - Feasible set for motion camouflage

Definition 4.2.1 *Given ϵ and τ, let $\mathcal{J}_\epsilon^\tau$ be defined as*

$$\mathcal{J}_\epsilon^\tau = \{\mu : \mu > 0,\ c_2(\mu, \tau, \epsilon) > \delta(\epsilon)\} \tag{4.42}$$

We say $\mathcal{J}_\epsilon^\tau$ is a feasible set for motion camouflage if $\mathcal{J}_\epsilon^\tau$ is not empty.

We are interested in the non emptiness of the set $\mathcal{J}_\epsilon^\tau$ for a given ϵ and τ. We analyze the quadratic inequality (4.38) and some key observations are listed below:

- The graph of the function $f(\mu) = \left[\mu\left(\frac{1-\nu}{1+\nu}\right) - \left(\frac{1+\nu}{r_0} + \frac{c_1}{\sqrt{\epsilon}}\right)\right]$ is a straight line (we refer to this line as $\mathtt{l}(\epsilon)$) with slope $\frac{1-\nu}{1+\nu} < 1$ and intersects the vertical

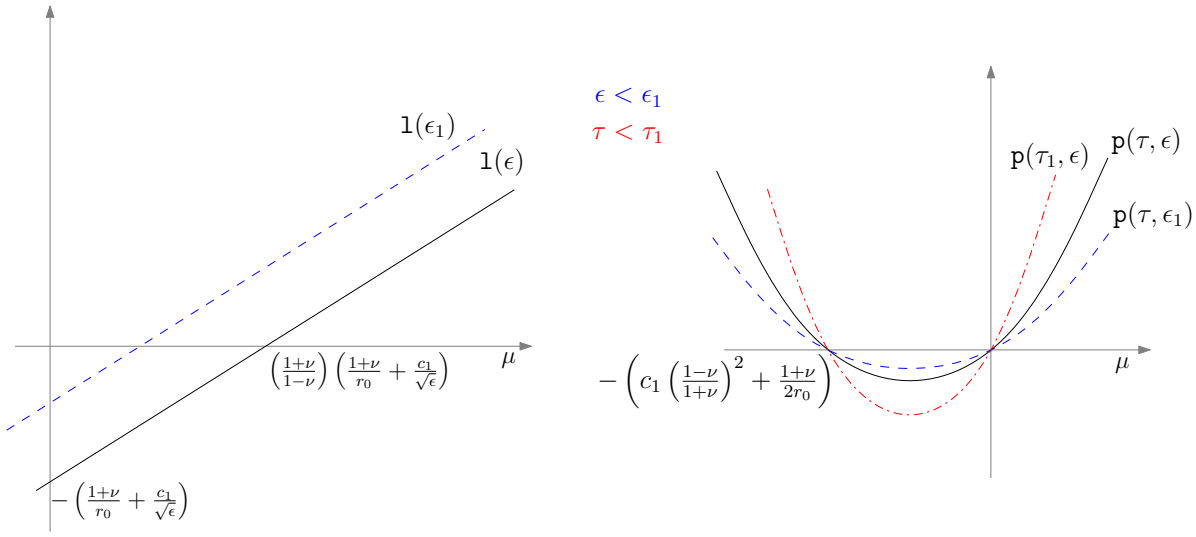

Figure 4.2: Figure (a): $\mathtt{l}(\epsilon)$ shifts towards right (left) side as ϵ decreases (increases). Figure (b): $\mathtt{p}(\tau, \epsilon)$ scales narrower (wider) with the decease (increase) in ϵ, the opposite scaling happens with the increase (decrease) in τ.

axis at $-\left(\frac{1+\nu}{r_0}+\frac{c_1}{\sqrt{\epsilon}}\right)$. Further, a decrease (increase) in ϵ would shift the line parallel to the right (left) side as shown in the figure (4.2(a)).

- The graph of the function $g(\mu)=\frac{\tau}{\sqrt{\epsilon}}\mu\left[c_1+\left(\frac{1+\nu}{1-\nu}\right)^2\left(\mu+\frac{1+\nu}{2\ r_0}\right)\right]$, is a parabola (we refer to this curve as $\mathtt{p}(\tau, \epsilon)$) passing through the origin and the point $\left(-\left(\frac{1+\nu}{2r_0}+c_1\left(\frac{1-\nu}{1+\nu}\right)^2\right), 0\right)$. Further, a decrease (increase) in ϵ, keeping τ fixed, would scale the parabola narrower (broader). Again, here, the parabola passes through the same points discussed above. However, an increase (decrease) in τ, keeping ϵ fixed, has the opposite scaling effect. These scaling effects are clearly shown in figure (4.2(b)).

- As can be seen from figure (4.3), if $\mathcal{J}_\epsilon^\tau \neq \phi$, $\overline{\mathcal{J}_\epsilon^\tau}$, for $\tau > 0$, is closed and bounded. *In the presence of delays the feasible set for motion camouflage is bounded.* However, for delay free case, i.e., $\tau = 0$, $\mathcal{J}_\epsilon^0$ represents the feasible

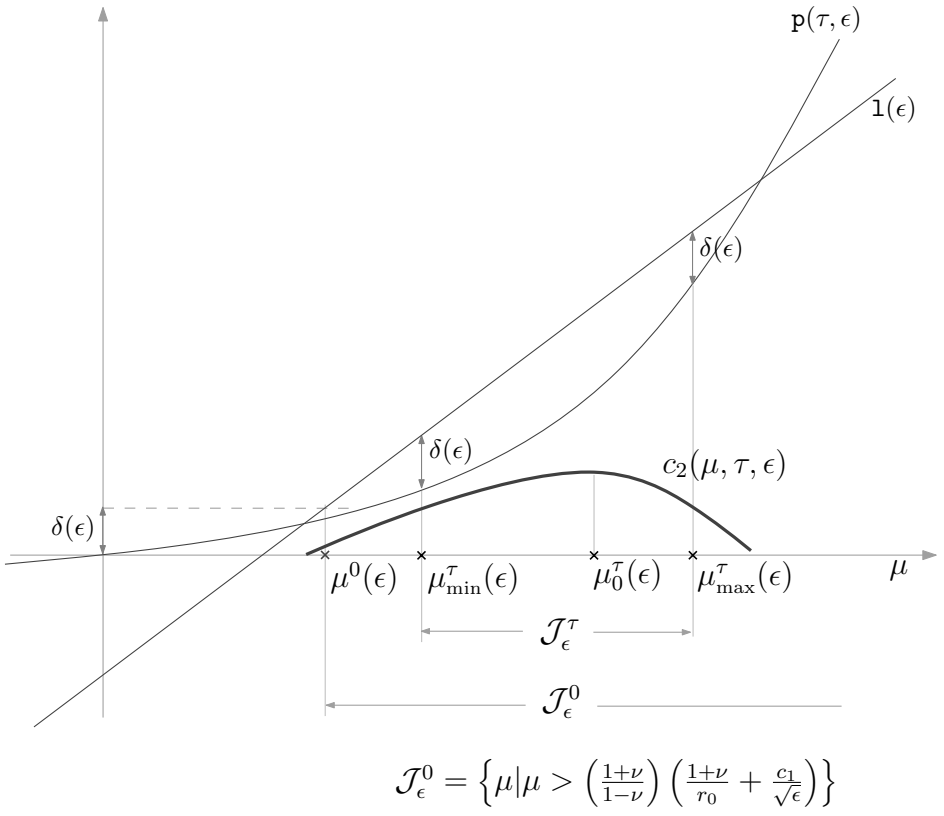

Figure 4.3: Feasible set for motion camouflage, $\mathcal{J}^\tau_\epsilon$, is bounded in the presence of delays.

set, which is defined as:

$$\mathcal{J}^0_\epsilon = \left\{\mu : \mu > 0, \mu > \left(\frac{1+\nu}{1-\nu}\right)\left(\frac{1+\nu}{r_0}+\frac{c_1}{\sqrt{\epsilon}}\right)\right\} \tag{4.43}$$

So, taking $\mu^0(\epsilon) = \left(\frac{1+\nu}{1-\nu}\right)\left(\frac{1+\nu}{r_0}+\frac{c_1}{\sqrt{\epsilon}}\right)$, we observe any $\mu > \mu^0(\epsilon)$ drives $\Gamma(t)$ close to $-1+\epsilon$ in finite time. *The feasible set for motion camouflage is unbounded in the absence of delays.*

- Further, as a nonempty $\overline{\mathcal{J}^\tau_\epsilon}$, $\tau > 0$, is compact,

$$\begin{aligned} \mu &\in (\mu^\tau_{min}(\epsilon),\ \mu^\tau_{max}(\epsilon))\,, \quad \forall \mu \in \mathcal{J}^\tau_\epsilon \text{ and} \\ 0 < \mu^0(\epsilon) &< \mu^\tau_{min}(\epsilon) < \mu < \mu^\tau_{max}(\epsilon) \end{aligned} \tag{4.44}$$

- Furthermore, $c_2(\mu, \tau, \epsilon)$ is a concave function on the compact set $\overline{\mathcal{J}_\epsilon^\tau}$. So, $c_2(\mu, \tau, \epsilon)$ has a unique maximum at $\mu_0^\tau(\epsilon)$ on $\overline{\mathcal{J}_\epsilon^\tau}$ (see figure (4.3)).

4.2.3.1 Variation of $\mathcal{J}_\epsilon^\tau$ with ϵ and τ

We observe how the feasible set $\mathcal{J}_\epsilon^\tau$ varies with respect to variations in ϵ and τ.

Variations with respect to ϵ: Keeping τ fixed, we observed earlier that if ϵ decreases (increases) the line $\mathtt{l}(\epsilon)$ shifts towards right (left) side and the parabola $\mathtt{p}(\tau, \epsilon)$ becomes narrower (wider). This affects the size of feasible set for motion camouflage. Let $\epsilon_1 > \epsilon_2$, due to the above variation of curves (see figure (4.4)),

$$\forall \mu > 0, c_2(\mu, \tau, \epsilon_1) > c_2(\mu, \tau, \epsilon_2). \tag{4.45}$$

Further, we know $\delta(\epsilon)$ is a monotone decreasing function, so for $\epsilon_1 > \epsilon_2 \;\; \delta(\epsilon_1) < \delta(\epsilon_2)$. Clearly,

$$\begin{aligned} \mu \in \mathcal{J}_{\epsilon_2}^\tau, \quad c_2(\mu, \tau, \epsilon_2) &> \delta(\epsilon_2) \\ c_2(\mu, \tau, \epsilon_1) &> c_2(\mu, \tau, \epsilon_2) > \delta(\epsilon_2) > \delta(\epsilon_1) \;\text{ and this implies }\; \mu \in \mathcal{J}_{\epsilon_1}^\tau \\ \mathcal{J}_{\epsilon_2}^\tau &\subset \mathcal{J}_{\epsilon_1}^\tau \end{aligned} \tag{4.46}$$

Keeping τ fixed, the feasible set for motion camouflage shrinks as ϵ decreases. Figure (4.4) summarizes the effect of ϵ on the feasible sets for feedback gain.

Variations with respect to τ: When ϵ is kept fixed, the line $\mathtt{l}(\epsilon)$ is fixed, and an

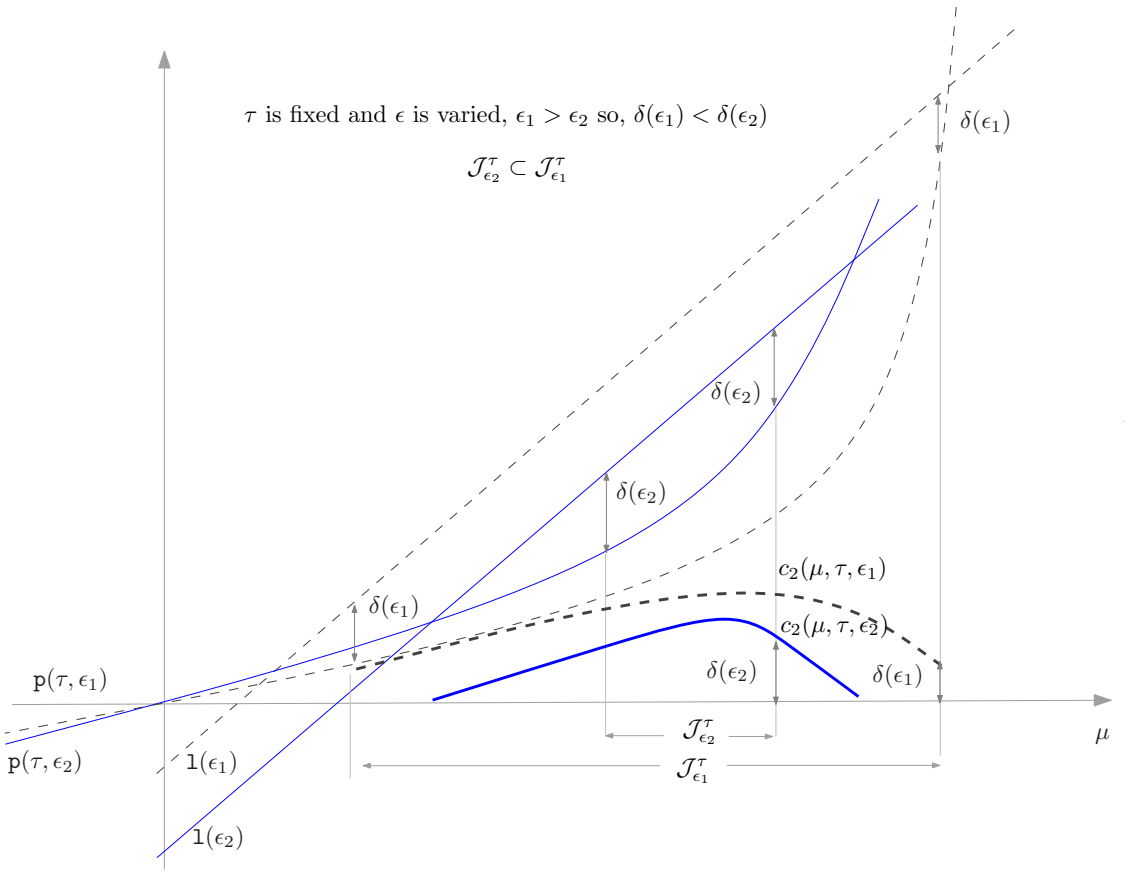

Figure 4.4: Variation of feasible sets with ϵ with fixed τ. The feasible sets shrink as ϵ decreases.

increase (decrease) in τ scales the parabola $\mathtt{p}(\tau, \epsilon)$ narrower (wider). This variation is captured in the figure (4.5). For $\tau_1 > \tau_2 > 0$, using the similar analysis, as above, we observe that

$$\mathcal{J}^{\tau_1}_{\epsilon} \subset \mathcal{J}^{\tau_2}_{\epsilon} \subset \mathcal{J}^{0}_{\epsilon}. \tag{4.47}$$

Keeping ϵ fixed, the feasible set for motion camouflage shrinks as delay increases. Furthermore, from figure (4.5) it is obvious that for a given ϵ as we increase τ, $\exists \tau_{max}(\epsilon) > 0$, such that $\forall \tau > \tau_{max}(\epsilon)$, $\mathcal{J}^{\tau}_{\epsilon} = \phi$. Clearly, *the peak deviation, ϵ, from the state of motion camouflage limits the delay that can be introduced in the system.*

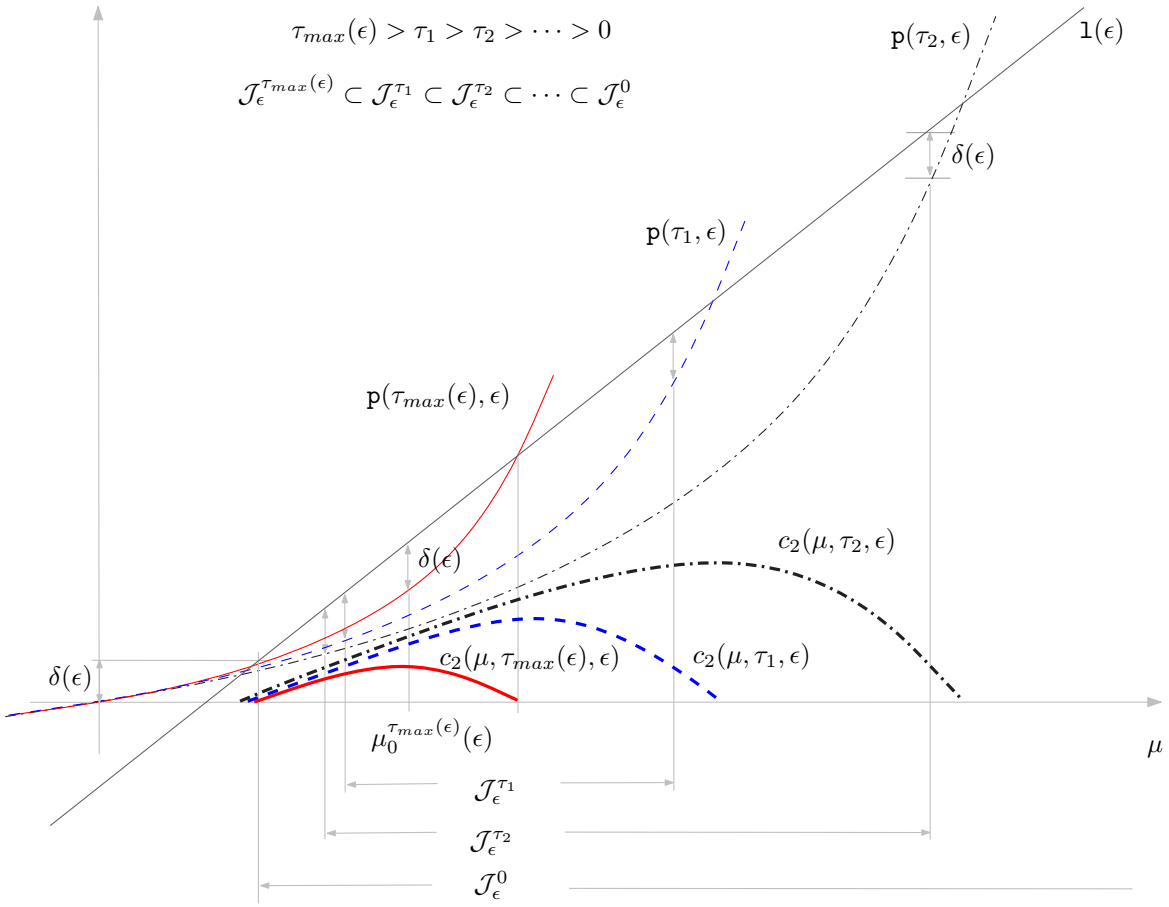

Figure 4.5: Variation of feasible sets with τ with fixed ϵ. There exists a maximum delay $\tau_{max}(\epsilon)$ and for any $\tau > \tau_{max}(\epsilon)$ reachability of a motion camouflage state is not guaranteed. Furthermore, for $\tau < \tau_{max}(\epsilon)$, the feasible sets shrink with the increase in τ.

So the feasible sets have the following relation

$$\phi = \mathcal{J}_\epsilon^{\tau} \subset \mathcal{J}_\epsilon^{\tau_{max}(\epsilon)} \cdots \subset \mathcal{J}_\epsilon^{\tau_1} \subset \mathcal{J}_\epsilon^{\tau_2} \cdots \subset \mathcal{J}_\epsilon^0$$
$$\text{for } \tau > \tau_{max}(\epsilon) > \cdots > \tau_1 > \tau_2 > \cdots > 0 \tag{4.48}$$

Now, we estimate $\tau_{max}(\epsilon)$ using the previous observations. As $c_2(\mu, \tau, \epsilon)$ is concave in μ on $\mathcal{J}_\epsilon^{\tau}$,

$$\max_{\mu \in \mathcal{J}_\epsilon^{\tau_{max}(\epsilon)}} c_2(\mu, \tau_{max}(\epsilon), \epsilon) = \delta(\epsilon). \tag{4.49}$$

Completing the squares we observe that an unique maximum is achieved at

$$\begin{aligned}\mu_0^{\tau_{max}(\epsilon)}(\epsilon) &= \frac{1}{2}\left[\frac{\sqrt{\epsilon}}{\tau_{max}(\epsilon)}\left(\frac{1-\nu}{1+\nu}\right)^3 - \left(c_1\left(\frac{1-\nu}{1+\nu}\right)^2 + \frac{1+\nu}{2r_0}\right)\right] \\ &= \frac{1}{2}\left(c_1\left(\frac{1-\nu}{1+\nu}\right)^2 + \frac{1+\nu}{2r_0}\right)\left(\frac{1}{\eta_{max}(\epsilon)} - 1\right) \qquad (4.50)\end{aligned}$$

where $\eta_{max}(\epsilon) = \frac{\tau_{max}(\epsilon)}{\sqrt{\epsilon}\ \xi_0}$ and

$$\xi_0 = \left(\frac{1-\nu}{1+\nu}\right)^3 \left(c_1\left(\frac{1-\nu}{1+\nu}\right)^2 + \frac{1+\nu}{2r_0}\right)^{-1}. \qquad (4.51)$$

As $\mu_0^{\tau_{max}(\epsilon)}(\epsilon) > 0$, an upper bound on the delay $\tau_{max}(\epsilon)$ is given by

$$\tau_{max}(\epsilon) < \sqrt{\epsilon}\ \xi_0 \qquad (4.52)$$

Using such a $\mu_0^{\tau_{max}(\epsilon)}(\epsilon)$, we have

$$c_2(\mu_0^{\tau_{max}(\epsilon)}(\epsilon), \tau_{max}(\epsilon), \epsilon) = \delta(\epsilon) \qquad (4.53)$$

$$\frac{\left[\frac{\tau_{max}(\epsilon)}{\sqrt{\epsilon}}\left(c_1 + \left(\frac{1+\nu}{1-\nu}\right)^2 \frac{1+\nu}{2r_0}\right) - \frac{1-\nu}{1+\nu}\right]^2}{4\frac{\tau_{max}(\epsilon)}{\sqrt{\epsilon}}\left(\frac{1+\nu}{1-\nu}\right)^2} - \left(\frac{1+\nu}{r_0} + \frac{c_1}{\sqrt{\epsilon}}\right) = \delta(\epsilon). \qquad (4.54)$$

We write (4.54) as a quadratic in $\tau_{max}(\epsilon)$ as

$$\begin{aligned}\left(\tau_{max}(\epsilon) - \sqrt{\epsilon}\ \xi_0\right)^2 &= 4\tau_{max}(\epsilon)\left(\frac{1+\nu}{1-\nu}\right)^4 \xi_0^2 \left(c_1 + \left(\frac{1+\nu}{r_0} + \delta(\epsilon)\right)\sqrt{\epsilon}\right) \\ &= 4\tau_{max}(\epsilon)\left(\beta + \gamma\sqrt{\epsilon}\right) \qquad (4.55)\end{aligned}$$

where $\beta = \xi_0^2 c_1 \left(\frac{1+\nu}{1-\nu}\right)^4$ and $\gamma = \xi_0^2 \left(\frac{1+\nu}{r_0} + \delta(\epsilon)\right) \left(\frac{1+\nu}{1-\nu}\right)^4$. We choose a particular root of the equation (4.55) for $\tau_{max}(\epsilon)$ so as to satisfy (4.52).

$$\begin{aligned}\tau_{max}(\epsilon) &= (\xi_0 + 2\gamma)\sqrt{\epsilon} + 2\beta \left(1 - \sqrt{1 + \frac{(\xi_0 + 2\gamma)\sqrt{\epsilon}}{\beta} + \left[\left(\frac{\xi_0 + 2\gamma}{2\beta}\right)^2 - \left(\frac{\xi_0}{2\beta}\right)^2\right]\epsilon}\right) \\ &= 2\beta \left[1 + \frac{(\xi_0 + 2\gamma)\sqrt{\epsilon}}{2\beta} - \sqrt{1 + \frac{(\xi_0 + 2\gamma)\sqrt{\epsilon}}{\beta} + \left[\left(\frac{\xi_0 + 2\gamma}{2\beta}\right)^2 - \left(\frac{\xi_0}{2\beta}\right)^2\right]\epsilon}\right].\end{aligned} \tag{4.56}$$

We write $\frac{\xi_0+2\gamma}{\beta}$ as,

$$\frac{\xi_0 + 2\gamma}{\beta} = \left(\frac{1-\nu}{1+\nu}\right)^3 + \left[\frac{5+3\nu}{2r_0} + 2\delta(\epsilon)\right] \frac{(1-\nu)^2}{\nu^2 u_{max}(1+\nu)} \tag{4.57}$$

If $(\xi_0 + 2\gamma)\sqrt{\epsilon} \ll \beta$, which is true with small ϵ, $\nu \to 1$, $|\mathbf{r}(0)| \gg r_0$, then the upper bound on the delay is approximately given as

$$\tau_{max}(\epsilon) \approxeq \frac{\xi_0^2 \epsilon}{4\beta} \tag{4.58}$$

Again, the feedback gain $\mu_0(\epsilon)$ that guarantees to drive $\Gamma(t)$ close to $-1+\epsilon$, in the presence of the largest delay $\tau_{max}(\epsilon)$, is given as

$$\mu_0^{\tau_{max}(\epsilon)}(\epsilon) = \frac{1}{2}\left(c_1 \left(\frac{1-\nu}{1+\nu}\right)^2 + \frac{1+\nu}{2r_0}\right)\left(\frac{1}{\eta_{max}(\epsilon)} - 1\right) \tag{4.59}$$

where

$$\eta_{max}(\epsilon) = \frac{\tau_{max}(\epsilon)}{\xi_0\sqrt{\epsilon}}. \tag{4.60}$$

If $(\xi_0 + 2\gamma)\sqrt{\epsilon} \ll \beta$, then

$$\eta_{max}(\epsilon) \approx \frac{\xi_0\sqrt{\epsilon}}{4\beta} \tag{4.61}$$

and using equation (4.51) the gain is approximated as

$$\begin{aligned}
\mu_0^{\tau_{max}(\epsilon)}(\epsilon) &\approx \frac{1}{2}\left(c_1\left(\frac{1-\nu}{1+\nu}\right)^2 + \frac{1+\nu}{2r_0}\right)\frac{1}{\eta_{max}(\epsilon)} \\
&= \frac{2\beta}{\xi_0\sqrt{\epsilon}}\left(c_1\left(\frac{1-\nu}{1+\nu}\right)^2 + \frac{1+\nu}{2r_0}\right) \\
&= \frac{2\xi_0 c_1}{\sqrt{\epsilon}}\left(\frac{1+\nu}{1-\nu}\right)^4\left(c_1\left(\frac{1-\nu}{1+\nu}\right)^2 + \frac{1+\nu}{2r_0}\right) \\
&= \frac{2c_1}{\sqrt{\epsilon}}\left(\frac{1+\nu}{1-\nu}\right)
\end{aligned} \tag{4.62}$$

Summary: We summarize the observations as follows:

- For delay free case, i.e., $\tau = 0$, the pursuer evader system can be driven arbitrary close to a state of motion camouflage ($\epsilon \to 0$), by increasing the feedback gain μ. Further, for a given ϵ, the peak deviation from the state of motion camouflage, the feasible set for motion camouflage $\mathcal{J}_\epsilon^0$ is given by $\left(-\left(\frac{1+\nu}{r_0} + \frac{c_1}{\sqrt{\epsilon}}\right), \infty\right)$. *In the absence of delays the feasible set for motion camouflage is unbounded.*

- In the presence of delays, it is possible to drive the system ϵ-close to a state of motion camouflage under certain conditions.

  – There exists an upper bound, $\tau_{max}(\epsilon)$, on the delay that can be intro-

duced in the system given by (4.56). *Motion camouflage is not possible if* $\tau > \tau_{max}(\epsilon)$.

– If $\tau < \tau_{max}(\epsilon)$, motion camouflage is possible and *the feasible set for motion camouflage is bounded*. Further,

$$\mathcal{J}_\epsilon^{\tau_{\max}(\epsilon)} \subset \mathcal{J}_\epsilon^{\tau_2} \subset \cdots \mathcal{J}_\epsilon^{\tau_1} \subset \mathcal{J}_\epsilon^{0} \quad \tau_{\max}(\epsilon) > \tau_2 > \cdots > \tau_1 > 0 \quad (4.63)$$

The feasible set for motion camouflage shrinks as the delay increases. In addition, there exists a gain $\mu_0^{\tau_{max}(\epsilon)}(\epsilon)$ that drives the system always to a state of motion camouflage given by equation (4.62).

4.3 Simulation results

Figure (4.6) illustrates the trajectories of the pursuer - evader system (4.2) and (4.4) under the control law (4.3) for the pursuer, and a constant steering control for the evader. When the baselines connecting the pursuer and evader are parallel over a time interval then $\Gamma = -1$, and the system is in a state of motion camouflage. We choose $\nu = 0.8$, $u_{max} = 0.25$, $r_0 = 5$ and $|\mathbf{r}(0)| = 75$ as the simulation parameters. We seek to illustrate the effect of sensorimotor/communication delay on reaching the state of motion camouflage. The peak deviation from the state of motion camouflage is taken as $\epsilon = \max(1 + \Gamma(t))$, for a particular choice of gain and delay. With zero delay, ϵ can be made arbitrary small by increasing the gain. This is clearly shown in figure (4.7). However, we notice that at very low values of gain the

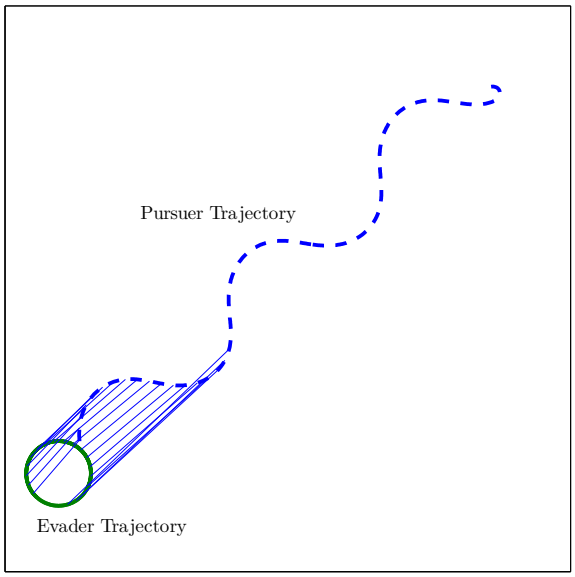

Figure 4.6: Evader trajectory with constant steering control (dark line) and the corresponding pursuer trajectory (dashed dark line), evolving according to (4.2) and (4.4), with pursuer control given by (4.3).

system fails to reach a state of motion camouflage even in the absence of delays. This observation is in agreement with the result that the feasible set for motion camouflage has a lower bound.

In the presence of delays, ϵ cannot be specified arbitrary small by simply increasing the gain. As shown in figure (4.7) only a range of values for μ would result in small ϵ. This clearly agrees with the observation that the feasible set for motion camouflage is bounded in the presence of delays. Furthermore, we clearly observe that feasible sets shrink with the increase in delay. Figure (4.8) shows the variation

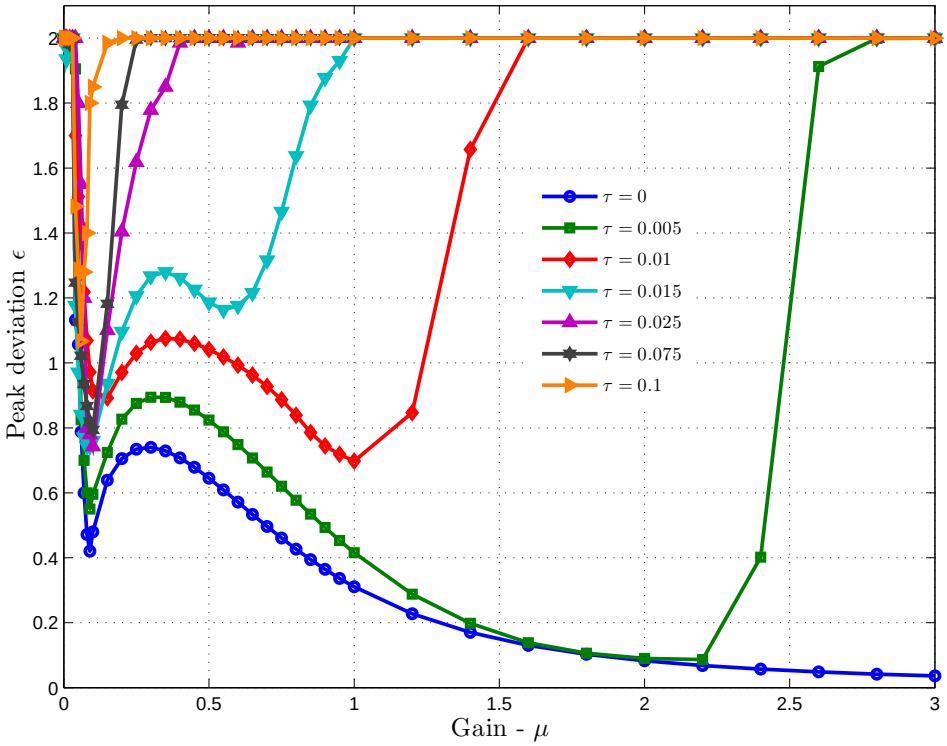

Figure 4.7: Peak deviation from motion camouflage (ϵ) is plotted as a function of increasing feedback gain in the presence of various delays.

of ϵ for different values of delay using a constant gain μ. Clearly, ϵ can be made arbitrary small by increasing the gain μ. However, for small ϵ, there exists a upper bound on the delay, $\tau_{max}(\epsilon)$, above which the system cannot be driven $\epsilon-$ close to a state of motion camouflage by any choice of gain. This observation is illustrated in figure (4.8), where the dotted line represents $\tau_{max}(\epsilon)$ and there does not exist a gain that can drive $\Gamma(t)$ close to $-1+\epsilon$ for $\tau > \tau_{max}(\epsilon)$. In addition, the line $\tau_{max}(\epsilon)$ varies linearly with ϵ, in agreement with (4.58). Figure (4.9) shows the variation of ϵ for different values of delay with fixed gain $\mu = 0.55$. Thus clearly the peak deviation increases as the delay is increased.

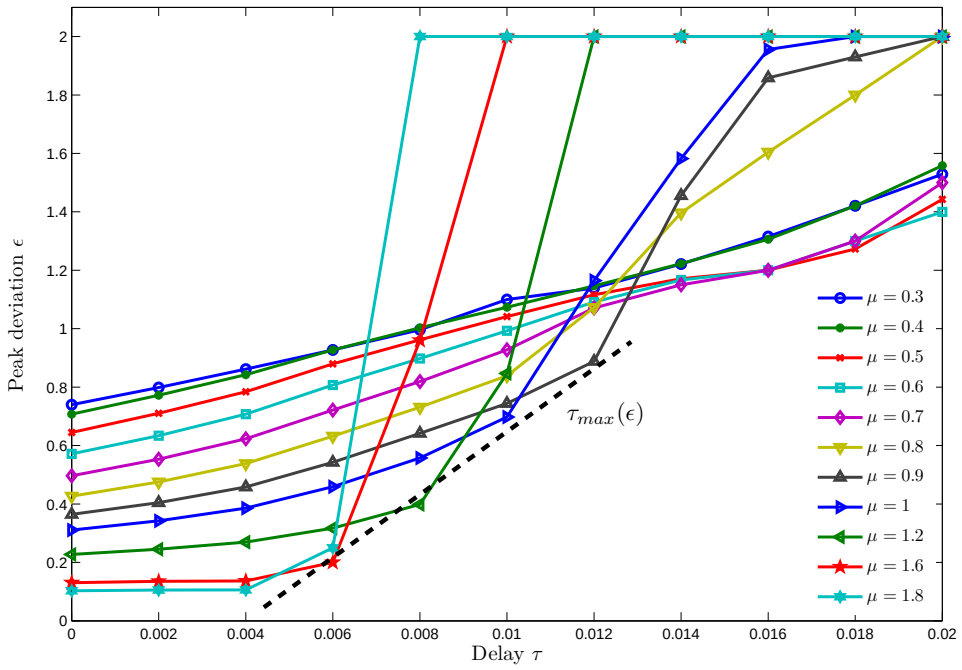

Figure 4.8: Peak deviation from motion camouflage (ϵ) is plotted as a function of increasing delay for various feedback gains. The dark dashed line corresponds to $\tau_{max}(\epsilon)$, an upper bound on the delay that can be introduced into the system for a given ϵ.

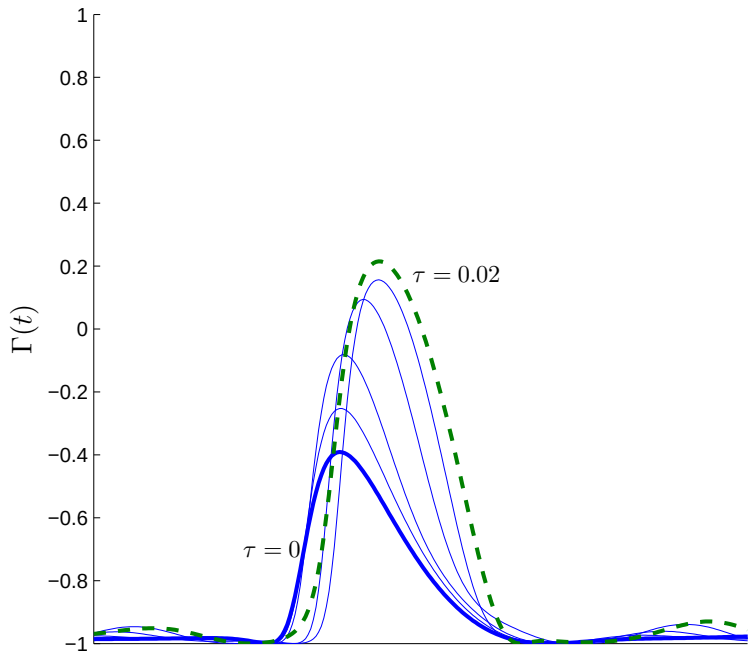

Figure 4.9: $\Gamma(t)$ is plotted as a function of time, for the pursuit illustrated in figure (4.6), in the presence of sensorimotor delays. Various traces correspond to increasing values of delay with a feedback gain $\mu = 0.55$, dark trace corresponds to $\tau = 0$ and dark dashed trace corresponds to $\tau = 0.02$ (times are included after Γ has come down to nearly -1).

Chapter 5

Conclusion & Future work

We began the thesis with a review of pursuit strategies seen in nature and engineering. We discuss a particular stealthy pursuit called motion camouflage with respect to a point at infinity. This strategy renders the baseline to be parallel. We review CATD strategy which also renders the baseline to be parallel. Thus both the strategies are geometrically indistinguishable.

For these strategies which result in same behavior (parallelism of the baseline), we hypothesize that the guidance laws used by the pursuer in the two strategies are identical. To validate the hypothesis we use experimental data obtained from real bat-insect encounters, where an echolocating bat uses CATD strategy during capture phase (refer to [GHKM06]). We develop a regularized inversion algorithm in chapter 2 to extract steering controls from uniformly sampled trajectory data. In addition, we present a numerically efficient algorithm to extract the controls. Since sensorimotor delays are inevitable, we modify the hypothesis taking delays into account. We develop a detailed methodology in chapter 3 to verify the modified hypothesis. The guidance laws in the two strategies are statistically identical with a great correlation (nearly 0.8). For the correlation plots mentioned in chapter 3, the variation of correlation is not very significant with the variation in delay around

optimal delay. There are several factors of variability that could affect this study. Firstly, the motion camouflage control laws drive the system to a state of motion camouflage under certain conditions, such as the speed of the evader is less than the speed of the pursuer, which is not true always. Further, the choice ATTACK region mentioned in chapter 3 could affect the correlation study. Identifying the factors of variability is important in validation studies and could be considered for future work.

We address the effect of delays on the performance of steering laws for motion camouflage. These delays are mainly due to sensorimotor processing and communication. We consider a planar setting for the analysis. We derive an upper bound of the delay that can be introduced in the system and the feasible values of feedback gain that can drive the system close to state of motion camouflage (in finite time). An extension to 3D case can be considered for future work.

Bibliography

[AM03] A. J. Anderson and P. W. McOwan. Model of a predatory stealth behavior camouflaging motion. *Proc. Royal Soc. B*, 270:489–495, 2003.

[Bis75] Richard L. Bishop. There is more than one way to frame a curve. *Amer. Math. Monthly*, 82(3):246–251, March 1975.

[Bro70] R. W. Brockett. *Finite Dimensional Linear Systems*. Series in Decision and Control. Wiley, Ney York, NY, 1^{st} edition, 1970.

[CFC04] N. E. Carey, J. J. Ford, and J.S. Chahl. Biologically inspired guidance for motion camouflage. In *Proc. Asian Control Conference*, volume 3, pages 1793–1799. IEEE, July 2004.

[CL75] T. S. Collett and M. F. Land. Visual control of flight behaviour in the hoverfly, syritta pipiens. *Journal of Comp. Physiol.*, 99:1–66, 1975.

[GHKM06] Kaushik Ghose, Timothy K. Horiuchi, P. S. Krishnaprasad, and Cynthia F. Moss. Echolocating bats use a nearly time-optimal strategy to intercept prey. *PLoS Biology*, 4(5):865–873, May 2006.

[Gle04] P. Glendinning. The mathematics of motion camouflage. *Proc. Royal Soc. B*, 271:477–481, 2004.

[GM06] Kaushik Ghose and Cynthia F. Moss. Steering by hearing: A bat's acoustic gaze is linked to its flight motor output by a delayed, adaptive linear law. *Journal of Neuroscience*, 26(6):1704–1710, 2006.

[Ise02] A. Iserles. Brief introduction to Lie-group methods. *SIAM, Proceedings in Applied Mathematics Series*, 2002.

[JK06] E. W. Justh and P. S. Krishnaprasad. Steering laws for motion camouflage. *Proc. Royal Soc. A*, 462(2076):3629–3643, Dec. 2006.

[KN71] M. S. Klamkin and D. J. Newman. Cyclic pursuit or 'the three bugs problem'. *Amer. Math. Monthly*, 78(6):631–639, June 1971.

[MBF04] J. A. Marshall, M. E. Broucke, and B. A. Francis. Formations of vehicles in cyclic pursuit. *IEEE Transactions on Automatic Control*, 49(11):19631974, 2004.

[MCS03] A. Mizutani, J. S. Chahl, and M. V. Srinivasan. Motion camouflage in dragonflies. *Nature*, 423:604, 2003.

[MS] Silvia Mastellone and Mark W. Spong. Stability and tracking with time-varying delay. *Systems and Control Letters*. Under review.

[MT74] Alex Mazanov and Keith P. Tognetti. Taylor series expansion of delay differential equations – A warning. *Jour. theor. Biol.*, 46:271–282, 1974.

[RJK06] P. V. Reddy, E. W. Justh, and P. S. Krishnaprasad. Motion camouflage in three dimensions. In *Proc. 45th IEEE Conf. Decision and Control*, pages 3327–3332. IEEE, Dec. 2006.

[SD95] M.V Srinivasan and M. Davey. Strategies for active camouflage of motion. *Proc. Royal Soc. B*, 259:19–25, 1995.

[Shn98] N. A. Shneydor. *Missile Guidance and Pursuit: Kinematics, Dynamics and Control*. Horwood publishing, Chichester, 1998.